

PHOTON AND NEUTRAL PION PRODUCTION IN D-AU COLLISIONS AT RHIC

Jean-François Paquet
Department of Physics
McGill University, Montréal

January 2011

A thesis submitted to McGill University in partial fulfillment of the
requirements of the degree of Master of Science

©Jean-François Paquet 2011

Contents

Résumé	v
Abstract	vi
Acknowledgements	vii
1 Introduction	1
1.1 Relativistic nuclear collisions	2
1.2 Hard particle production	4
1.3 Deuteron-gold collisions	6
2 Theory	8
2.1 Theories of fundamental interactions	8
2.1.1 QCD	9
2.1.2 Standard Model	12
2.2 From theory to experiments	13
2.2.1 S-matrix formalism	14
2.2.2 Perturbative QCD	14
3 Hard π^0 and photon production in proton-proton collisions	19
3.1 Leading order cross-section	21
3.1.1 π^0	23
3.1.2 Photons	27
3.2 Next-to-leading order	27
4 Hard π^0 and photon production in deuteron-gold collisions	31
4.1 Collisions according to the Glauber model	32
4.1.1 Binary scaling	34
4.2 Deuteron-gold collisions and nuclear effects	35

4.2.1	Nuclear modification factor and the isospin effect	37
4.2.2	Nuclear parton distribution functions	40
4.3	Comparison with data	42
5	Hard parton energy loss in deuteron-gold collisions	47
5.1	Simple model of parton energy loss	50
5.2	Comparison with another model of energy loss	52
5.3	Analysis	54
6	Conclusion	56

List of Figures

1.1	Definition of the transverse plane with respect to the collision axis and a sketch of a proton-proton collision	4
1.2	A proton-proton collision according to the parton model	5
2.1	Running of $\alpha_s(Q)$ compared with experimental measurements	11
3.1	π^0 differential cross-section in proton-proton collisions at $\sqrt{s} = 200$ GeV and midrapidity compared to leading order calculations. $\alpha_s(M_Z) = 0.130$	24
3.2	π^0 differential cross-section in proton-proton collisions at $\sqrt{s} = 200$ GeV and midrapidity compared to leading order calculations. $\alpha_s(M_Z) = 0.1181$	24
3.3	Photon differential cross-section in proton-proton collisions at $\sqrt{s} = 200$ GeV and midrapidity compared to leading order calculations. $\alpha_s(M_Z) = 0.130$	26
3.4	Separate fragmentation and isolated leading order calculations of photon differential cross-section in proton-proton collisions	26
3.5	π^0 differential cross-section in proton-proton collisions at $\sqrt{s} = 200$ GeV and midrapidity compared to next-to-leading order calculations	28
3.6	Photon differential cross-section in proton-proton collisions at $\sqrt{s} = 200$ GeV and midrapidity compared to next-to-leading order calculations	29
3.7	Photon differential cross-section in proton-proton collisions compared to separate isolated and fragmentation next-to-leading order calculations	29
4.1	Geometry of a nucleus-nucleus collision	32
4.2	Scaling with A of the isospin-corrected Drell-Yan cross-section for various proton-nucleus collisions	35
4.3	π^0 differential cross-section in minimum bias deuteron-gold collisions at $\sqrt{s_{NN}} = 200$ GeV and midrapidity compared to scaled proton-proton calculations	36
4.4	Photon differential cross-section in minimum bias deuteron-gold collisions at $\sqrt{s_{NN}} = 200$ GeV and midrapidity compared to scaled proton-proton calculations	36

4.5	$\langle R_{dAu} \rangle_{\text{MB}}$ for π^0 compared to isospin-corrected calculations . . .	38
4.6	$\langle R_{dAu} \rangle_{\text{MB}}$ for photons compared to isospin-corrected calculations	38
4.7	$\langle R_{dAu} \rangle_{\text{MB}}$ for π^0 compared to leading order calculations with EKS98 and EPS09 and next-to-leading order calculation with EPS09	43
4.8	$\langle R_{dAu} \rangle_{\text{MB}}$ for π^0 compared to calculations with HKN07 and EPS09 nuclear p.d.f.'s	44
4.9	$\langle R_{dAu} \rangle_{\text{MB}}$ for photons compared to calculations with HKN07 and EPS09 nuclear p.d.f.'s	44
5.1	Schematic comparison of hadron-hadron and nucleus-nucleus collisions	48
5.2	$\langle R_{dAu} \rangle_{\text{MB}}$ for π^0 calculated with EPS09 nuclear p.d.f. and simple parton energy loss	49
5.3	$\langle R_{dAu} \rangle_{\text{MB}}$ for π^0 calculated with HKN07 nuclear p.d.f. and simple parton energy loss	49
5.4	$\langle R_{dAu} \rangle_{\text{MB}}$ for photons calculated with EPS09 nuclear p.d.f. and simple parton energy loss	51
5.5	$\langle R_{dAu} \rangle_{\text{MB}}$ for photons calculated with HKN07 nuclear p.d.f. and simple parton energy loss	51
5.6	Diagrammatic comparison of hadron-nucleus collisions and semi- inclusive nuclear deep-inelastic scattering	53
5.7	Graphical extraction of energy loss parameter E_0	54

Résumé

La section efficace des photons et des pions neutres ayant de grandes quantités de mouvement transversales produits dans des collisions proton-proton est calculée en utilisant la formule standard basée sur la chromodynamique quantique (QCD) perturbative. Les calculs sont faits au premier “twist” et au second ordre, et sont comparés à des mesures provenant du *Relativistic Heavy Ion Collider* (RHIC). La section efficace est aussi calculée pour des collisions deutéron-or à l’aide d’un modèle basé sur des distributions de partons nucléaires et sur un prolongement de la formule des collisions proton-proton aux collisions noyau-noyau. Les calculs basés sur ce modèle sont comparés à des mesures provenant du même accélérateur. L’effet des pertes d’énergie des partons sur les calculs de sections efficaces dans les collisions deutéron-or est aussi étudié.

Abstract

The cross-section of large transverse momentum photons and neutral pions in proton-proton collisions is calculated using the standard perturbative QCD formula at leading twist, next-to-leading order, and is compared to data from the Relativistic Heavy Ion Collider (RHIC). The cross-section of hard photons and neutral pions is also calculated for deuteron-gold collisions using a model based on an extension of the proton-proton calculation to nucleus-nucleus collisions and on phenomenological nuclear parton distribution functions. The deuteron-gold calculations are compared to data measured at the same collider. The effect of parton energy loss on the deuteron-gold calculations is also investigated.

Acknowledgements

I first want to thank Charles Gale, my supervisor, for his help, his guidance and his patience. I also want to thank Björn Schenke for his invaluable help throughout my Master's Degree; important parts of this thesis would not have been possible without his assistance. I thank GuangYou Qin for his precious help during the early and later phase of my work. Finally, I thank Marius Cautun, Gojko Vujanovic, Jonathan Coull and Michael Richard for interesting discussions, and Paul Mercure for technical help.

Chapter 1

Introduction

The contribution of particle accelerators to high-energy physics is enormous. They provided the first insights of new physics, and plenty of data against which the new theories could be tested. In a way, their contribution can be likened to that of spectroscopy, a century ago, to the nascent field of quantum mechanics.

Data collected with increasingly sophisticated particle accelerators and detectors have helped establish the current theory of strong, weak and electromagnetic interactions, known as the Standard Model of particle physics. The latest accelerators are also expected to help developing the next generation of theories that will describe even better the interactions of elementary particles.

Beside looking for a replacement to the Standard Model, particle accelerators are also unique tools to *study* the Standard Model, which does not reveal its secrets easily. Particle accelerators are helping understanding the Standard Model just as much as they helped establishing it.

Colliding different kinds of particles together provides different kinds of information about elementary particles and their interactions. For example, in the past, highly inelastic collisions of high-energy electrons with protons (deep inelastic scattering — DIS) gave the first direct evidence of the existence of quarks and of their basic properties, while electron-positron (e^-e^+) collisions helped to firmly establish the existence of gluons and their role as carrier of the strong force [1, Section VI-A].

The type and amount of information that can be extracted from collisions also depend heavily on the capacities of the detectors that surround the region of the collisions. While the first experiments with high-energy electron-proton collisions could detect only the energy lost and the change of momentum of

the electron [2, Section III], modern detectors can also measure the energy and momentum of a large number of other particles — photons, hadrons, muons, ... — and also have a much better accuracy and an increased angle coverage¹, allowing more complex observables to be studied.

Hadronic collisions are fundamentally different from those involving leptons: in the first case, it is through the strong interaction that the colliding particles interact, while in the second case it is either through the electromagnetic or weak interaction. Relativistic nuclear collisions — collisions of nuclei at very high energies — have proved to be a very rich field of research and an excellent way of studying strong interactions. Such collisions are, however, much more complicated than e.g. electron-proton or e^-e^+ collisions.

1.1 Relativistic nuclear collisions

What makes relativistic nucleus-nucleus collisions, even proton-proton ones, so complicated is that while electrons are elementary particles, protons are not: they are composite objects of a very large number of quarks, antiquarks and gluons. A simple way of picturing an electron-proton collision is an electron that interacts electromagnetically with a single quark, antiquark or gluon (collectively known as partons). In the same picture, a simple proton-proton collision is actually a collision of two clouds of hundreds of partons. The partons may interact many times before they are bound together again into hadrons.

In collisions of larger nuclei — relativistic *heavy ion* collisions — even more partons interact. When the energy and the density of partons are high enough, the behaviour of the partons changes drastically: they start behaving like a plasma of almost free quarks and gluons — a quark-gluon plasma (QGP) [4]. For now, only in collisions of fairly large nuclei are the density and energy high enough for a QGP to be created, and only for a very short time. This is, however, a major discovery as the QGP is thought to be a new phase of matter that may have been the state of the Universe very shortly after the Big Bang.

The QGP is one of many discoveries made by particle accelerators recently. Interest in it has been especially high lately due to new results made available

¹See for example [3, Section 2] for a short description of the H1 and ZEUS detectors of the HERA accelerator.

thanks to the Relativistic Heavy Ion Collider (RHIC), a particle accelerator located at the Brookhaven National Laboratory built specifically to study collisions of heavy nuclei and to learn more about the QGP.

Even in collisions of very heavy nuclei at very high energies, a QGP is formed only in a tiny region of space for a very short period of time.² It is thus very challenging to learn about its properties. Most of the current techniques to do so are indirect and mostly based on the good understanding of relativistic nuclear collisions in which no QGP is expected to be formed, like proton-proton, proton-nucleus or light nuclei collisions, or even collisions of large nuclei at low energies. The core idea behind these indirect techniques is to use observables that are already well-understood in QGP-less nucleus-nucleus collisions as probes of the QGP: if a model that can describe a given observable in a QGP-less nucleus-nucleus collision has to be modified to describe the same observable in a collision where a QGP is created, then the required modifications to the model can be related to properties of the QGP. Of course, these indirect techniques require that QGP-less nucleus-nucleus collisions be very well understood, or at least that the observables used to study the QGP be well understood in such collisions.

In this thesis, a single observable is studied for two different collisions: hard particle production in relativistic proton-proton and deuteron-gold collisions. As hard particle production is one of the probes used to learn about the QGP in heavy ion collisions, it is possible to justify this whole thesis by the need to improve, or verify, our understanding of that observable in QGP-less nucleus-nucleus collisions. This is definitively one of the rationales of this thesis — an important one — but it would be unfair to say that it is the only one. Relativistic nuclear collisions, even simple proton-proton ones, offer countless opportunities to study strongly interacting particles and their interactions, and collisions like deuteron-gold ones add to these possibilities a window into the gold nucleus, without the complications of heavy ion collisions, that opens doors to many other applications.

²The dimensions and the lifetime of the QGP at RHIC are estimated to be of the *order* of fm (10^{-15} m) in size and fm/c ($\approx 3 \times 10^{-24}$ s) in time.

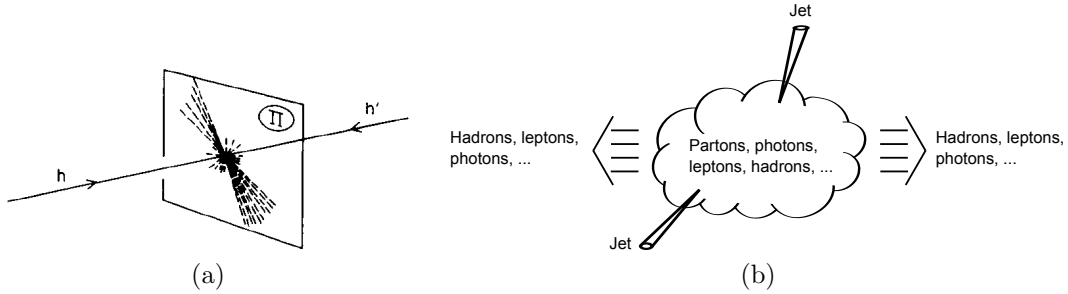


Figure 1.1: **a)** Definition of the transverse plane (identified by the letter Π) with respect to the collision axis and **b)** a sketch of a proton-proton collision. Figure 1.1a modified from [5, Figure 53]

1.2 Hard particle production

From an experimental point of view, a hard particle is a particle that has a large momentum and that is produced at a large angle with respect to the collision axis. This is usually summarised as “large transverse momentum”, where “transverse” refers to the *transverse plane*, shown in figure 1.1a: it is the plane perpendicular to the collision axis. The meaning of “large” in “large momentum” is not always well-defined, but it usually means a momentum larger than a few (1–5) GeV/c.

Hard hadrons produced in relativistic nuclear collisions are produced along with a group of hadrons moving roughly in the same direction but with a range of different momenta. This group of hadrons is called a *jet*. Figure 1.1b is a sketch of a nuclear collision with jets, depicted as cones, emerging from it.

The reason that makes hard hadrons, or hard particles in general, especially interesting is a theoretical one. To understand it, it is useful to describe the production of hard particles in a collision, a proton-proton collision for example, using what is called the parton model. In this model, hadrons are described as clouds of partons and collisions of hadrons are related to much simpler collisions of partons. Figure 1.2 shows a proton-proton collision according to this model.

Figure 1.2a shows the protons as clouds of partons. Figure 1.2b just shows that the collision is thus reduced to parton-parton interactions. Figure 1.2c illustrates a more interesting process, fragmentation. Fragmentation reflects the fact that partons are never detected alone, they are always bound into hadrons. Thus the partons exiting from the parton-parton interaction of figure 1.2b must somehow transform into hadrons; fragmentation represents this

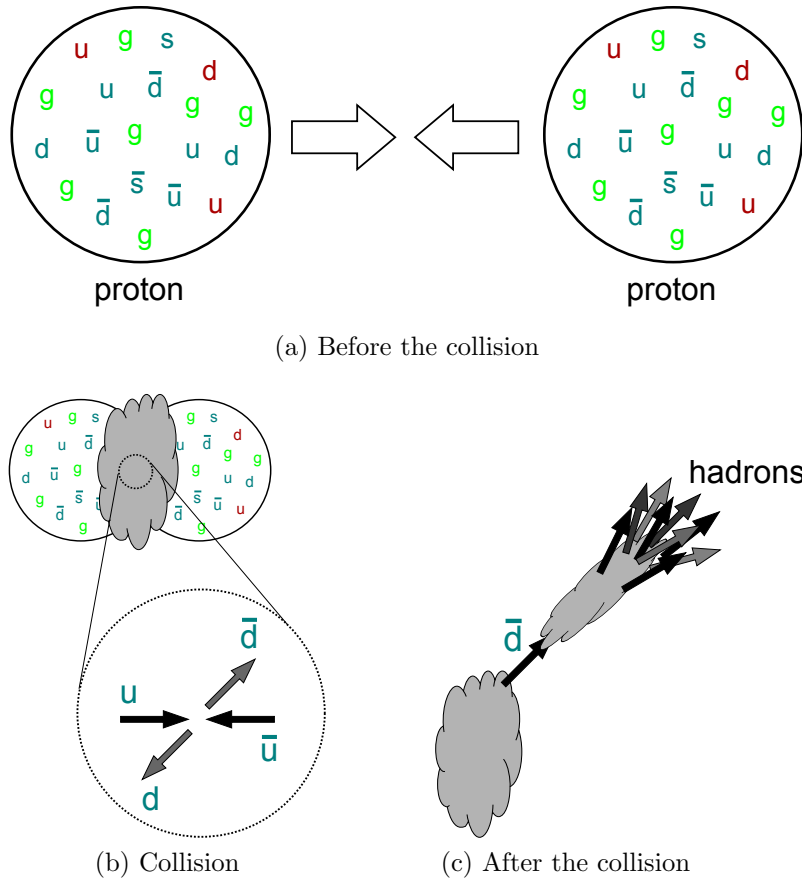


Figure 1.2: A proton-proton collision according to the parton model

process.

The parton model preceded the development of quantum chromodynamics (QCD), the current theory of strong interactions. It was developed using general physical arguments that were expected to hold when the momentum exchange of the parton-parton interaction (figure 1.2b) is large³, as in hard particle production. The parton model’s ability to describe data was often unsatisfactory, but it did allow to make a number of impressive predictions and it provided a very useful “intuitive” description of particle collisions that is still commonly used.

Attempts to formalise the parton model using quantum chromodynamics

³Although “large momentum exchange” and “large transverse momentum” are often used as synonyms, there is a nuance between the two that should be understood. The problem is that on the experimental side, it is difficult to know if a large momentum was exchanged in a parton-parton interaction. However, under the approximate assumption that the partons of a proton have no initial transverse momentum, if the transverse momentum of a produced particle is large, it *had* to emerge from a parton-parton collision that exchanged a large momentum (it is assumed that there is no other way for the particle to acquire a large transverse momentum).

yielded a framework called “perturbative QCD”. This new approach, widely used today, is able to describe data to an impressive precision. Yet perturbative QCD still has the same limitation as the parton model: it works only for large transverse momentum particles. The origin of this limitation is now well understood, it has to do with something called the running of the effective coupling, an intrinsic property of QCD. It is this property that makes possible the calculation of the cross-section of hard particles, but also that renders extremely challenging the same task for non-hard — that is, soft — particles. What sets hard particles apart from others is merely this ability to calculate their cross-section with perturbative QCD.

1.3 Deuteron-gold collisions

The framework of perturbative QCD that works so well for hard particle production in proton-proton collisions cannot be easily extended to nucleus-nucleus collisions like deuteron-gold ones.⁴ Actually, it is not yet known how to calculate hard particle production in nucleus-nucleus collisions *directly* from quantum chromodynamics. On the other hand, there are models, based to various extent on QCD, that can reproduce the data well. A model that can be used to calculate hard particle production in nucleus-nucleus collisions *in which no QGP is created* is described in chapter 4. The presence of a QGP renders the collisions much more complex and a significant amount of additional modeling is required; studying such collisions is a whole other story, not covered in this thesis.

As the QGP is studied at RHIC using relativistic gold-gold collisions, deuteron-gold collisions are a very important intermediate step in the quest to learn about the properties of the QGP. The theoretical understanding of deuteron-gold collisions is already much poorer than it is for proton-proton collisions, but deuteron-gold collisions are still significantly simpler than gold-gold collisions. They are thus very important to verify our understanding of e.g. hard particle production in such QGP-less collisions. They can also be

⁴Relativistic nuclear collisions are often classified as hadron-hadron, hadron-nucleus or nucleus-nucleus collisions. However, for hard particle production, the difference between hadron-nucleus collisions and nucleus-nucleus ones is less relevant than the formation or not of a QGP in those collisions. Thus, deuteron-gold collisions are treated here as nucleus-nucleus collisions, though in the classification scheme mentioned above they are closer to the hadron-nucleus category than the nucleus-nucleus one.

used as a simpler framework to test models necessary to understand heavy ion collisions, like parton energy loss models.

This thesis focuses on understanding well hard particle production in relativistic deuteron-gold collisions, not on the applications of this understanding. Only two types of particles are investigated: photons and neutral pions (π^0). The choice of π^0 among all the possible mesons is largely due to experimental factors: π^0 data are in general more widely available and more precise. For photons, the reasons are rather different: they are chosen because they provide channels of informations that are, if not complementary, at least different than those of mesons (and hadrons in general), as photons are elementary particles and are not affected by the strong force.

The structure of the thesis is as follow. The second chapter is devoted to explaining how hard particle cross-sections can be calculated from the Standard Model. Hard photon and π^0 production is explained in the third chapter for proton-proton collisions, and in the fourth chapter for deuteron-gold collisions. In both cases, the calculations are compared to data from RHIC.

The conclusions of the third chapter are fairly rigorous, based directly on quantum chromodynamics, but what is described in chapter 4 is really a *model*, one that was chosen among many other competing models. The possibility of adding parton energy loss to the model described in the fourth chapter is explored briefly in the fifth and final chapter of this thesis.

Chapter 2

Theory

A complex machinery is required to relate the current theory of weak, electromagnetic and strong interactions, the Standard Model, to quantities measurable in experiments. In this thesis, the only experimental results used are cross-sections measured by particle detectors in particle accelerators. This chapter is devoted to explaining how certain cross-sections can be calculated from the Standard Model. To do so, it is necessary to begin with a description of the latter.

2.1 Theories of fundamental interactions

The Standard Model is a theory that describes in a unified way the strong, weak and electromagnetic forces. The first step in this unification was the development of quantum electrodynamics (QED), a theory of electromagnetism compatible with quantum mechanics. A new theory that could describe both QED and the weak interaction was developed later, the electroweak theory. When a theory of strong interactions, quantum chromodynamics (QCD), was found some years later, it was combined with the electroweak theory to give what is now known as the Standard Model.

All these theories are variations of a larger group called quantum field theories. Quantum field theories describe the behaviour of “fields” in a way consistent with special relativity and quantum mechanics. A field is associated with every type of elementary particles, and an arbitrary number of elementary particles of a given type can be described with a single field. For example, the most basic form of QED consists of an electron field and a photon field, and it

can describe any low-energy system composed only of electrons and photons.¹

Quantum field theories differ by their field content — the number and type of fields that are included in each theory — and by how the fields are allowed to interact with each other. In a subset of quantum field theories called gauge theories, the ways fields are allowed to interact are restricted by requiring them to respect a certain symmetry, called the gauge symmetry. Quantum electrodynamics, quantum chromodynamics and the electroweak model are all gauge theories, with different field content and gauge symmetries.

Physical quantities can be calculated from the Lagrangian density of a quantum field theory. This Lagrangian density is defined by all possible combinations of fields that are consistent with Lorentz invariance (special relativity), the assumed gauge symmetry (for gauge theories) and a further restriction, renormalisability. For the present discussion, it is enough to say that renormalisability puts constraints on the dimension of the terms that can appear in the Lagrangian density. Although renormalisability is taken here as an assumption, it is really more a consequence of trying to describe with a quantum field theory a high-energy theory at low energies [7, Section 4.1].

Using the above three conditions, it is possible to write down the Lagrangian density of a gauge theory. Quantum chromodynamics, described in the next section, gives a good example of how it is done.

2.1.1 QCD²

Quantum chromodynamics is the theory of strong interactions. It describes the interactions of quarks and gluons. There are six “flavours” of quarks: up, down, strange, charm, top and bottom. There are also three “colours” of quarks, which can be labelled red, green and blue. There are thus 18 different types of quarks: red up quarks, red down quarks, green up quarks, . . . This means 18 fields. Quarks are spin-one-half fermions and as such are represented by Dirac fields, noted ψ_ρ . All the quark fields can be noted as one field using a tensor notation: $\psi_{\rho af}$ where “a” is a colour index and “f” a flavour one.

There are also 8 types of gluons, which are spin-one bosons each represented by a vector field, noted A_μ . All gluon fields can be noted as A_μ^α where the α

¹The low-energy constraint comes from the fact that at high enough energy, new types of particles can be created in the system. See [6, Section 1.2.2]. Also, there are actually three other fields, one for each neutrino, but they do not interact with electrons and photons. See [6, Section 1.6.1].

²This section is in large part based on [8, Section 2.1] and [6, Section 1.6.3].

index can take 8 values. The field content of QCD is thus 18 quark fields, $\psi_{\rho af}$, and 8 gluon fields, A_μ^α .

Quantum chromodynamics is a gauge theory, so the physics it describes is assumed to be invariant under a gauge symmetry. For QCD, this symmetry is assumed to be a symmetry under a mixing among its colours of each flavour of quarks. The mixing is assumed to be of the form

$$\begin{bmatrix} q'_r \\ q'_g \\ q'_b \end{bmatrix} = M \begin{bmatrix} q_r \\ q_g \\ q_b \end{bmatrix}$$

with $M^\dagger = M^{-1}$, for all six flavours of quarks. The transformation is assumed to be the same for every flavour.

A 3×3 matrix M that respects $M^\dagger = M^{-1}$ is an unitary matrix that can be written as $M = e^{i\theta} N$. N can be further decomposed as the exponential of a weighted sum of eight matrices Λ_α : $N = e^{i\omega_\alpha \Lambda_\alpha}$. The Λ_α matrices obey the relation $[\Lambda_\alpha, \Lambda_\beta] = if_{\alpha\beta\gamma} \Lambda_\gamma$. The decomposition of N in Λ_α and the relation obeyed by the Λ_α matrices can be better understood in the context of group theory, not used here. It comes from the fact that the Λ_α matrices form a representation of the $SU(3)$ group.

A term of the form $\bar{\psi}_{\rho af} (\not{D} + m) \psi_{\rho af}$, with $D_\mu = \partial_\mu - ig_s A_\mu^\alpha \Lambda_\alpha$, is assumed to appear in the Lagrangian density. This imposes that if the quark fields rotate in the colour space, the gluon fields also change in a well-defined way so that the term is left unchanged. This defines how the gluon fields transform because of the gauge symmetry, and it in turn imposes restrictions on the kind of terms involving those fields that can appear in the Lagrangian density.

The only other renormalisable, Lorentz invariant term compatible with the gauge symmetry is $G_{\mu\nu}^\alpha G^{\alpha\mu\nu}$ with $G_{\mu\nu}^\alpha \equiv \partial_\mu A_\nu^\alpha - \partial_\nu A_\mu^\alpha + g_s f_{\alpha\beta\gamma} A_\mu^\beta A_\nu^\gamma$.

The Lagrangian density of QCD is thus

$$\mathcal{L}_{\text{QCD}} = -\bar{\psi}_{\rho af} (\not{D} + m) \psi_{\rho af} - \frac{1}{4} G_{\mu\nu}^\alpha G^{\alpha\mu\nu} \quad (2.1)$$

Effective coupling and asymptotic freedom

Attempts to extract experimentally measurable quantities from QCD often result in calculations that seem to diverge. Some of those divergences are the result of inappropriate approximations made in the calculations, but one type of divergences, ultra-violet ones, is actually intrinsic to QCD [8, Section 3.2].

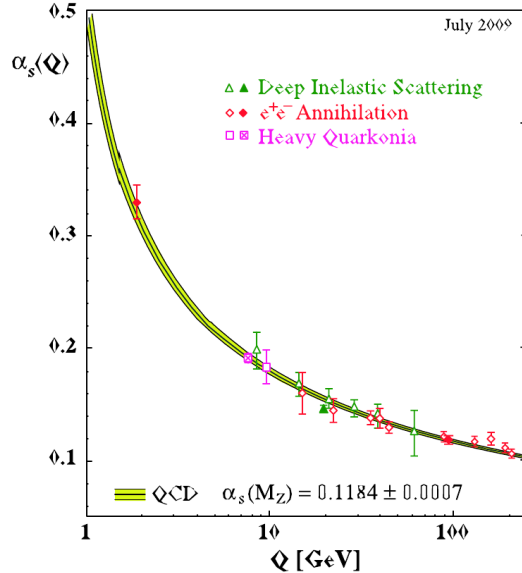


Figure 2.1: Running of $\alpha_s(Q)$ compared with experimental measurements. Figure from [9, Figure 5]

Two procedures must be applied to eliminate those divergences, regularisation and renormalisation. One of the results of renormalisation is the definition of an *effective* coupling constant³, $g_s(Q)$, that depends on an arbitrary energy scale, Q , the renormalisation scale. The Q evolution of $g_s(Q)$ is given by

$$Q \frac{dg_s(Q)}{dQ} = \beta(g_s(Q)) \quad (2.2)$$

where $\beta(g_s(Q))$ is called the beta function. What is very interesting is that $\beta(g_s(Q))$ can be calculated perturbatively and such calculations show that it is negative at large Q . This means that $g_s(Q)$ goes to zero as Q goes to infinity. This is called asymptotic freedom. It is a key in understanding why QCD interactions are very strong at low energies but seem to be weak at high energies. The evolution of $\alpha_s(Q)$, usually referred to as “the running of the coupling”, is illustrated in figure 2.1.⁴

Since equation 2.2 is a differential equation, it needs an initial condition to be solved. A common initial condition is $\alpha_s(M_Z)$, where $M_Z \approx$

³ $\alpha_s(Q) = g_s^2(Q)/4\pi$ is often used instead of $g_s(Q)$ as effective strong coupling constant.

⁴The procedure of renormalisation is not unique and it is possible to define $\alpha_s(Q)$ in many different ways. Figure 2.1 corresponds to a very specific definition of $\alpha_s(Q)$, and it is important to understand that the plot would be different for other definitions of $\alpha_s(Q)$. See the legend of [9, Figure 5] and the paper in general for the details on the definition used for figure 2.1.

91.19 GeV/c² [10, Section 1] is the mass of the Z boson. Another possible way of specifying the initial condition is Λ_{QCD} , which is the energy scale Q at which $\alpha_s(Q)$ diverges if the beta function is computed only at the first order.⁵

2.1.2 Standard Model

Quantum chromodynamics is one part of the Standard Model, the other being the electroweak theory. The particle content of the Standard Model is the quarks and gluons of QCD plus six spin-one-half fermions (electron, muon, tau, electron neutrino, mu neutrino and tau neutrino), four spin-one bosons ($W_\mu^1, W_\mu^2, W_\mu^3$ and B_μ) and the famous spin-zero Higgs boson [6, Chapter 2]. The observed bosons (W_μ^\pm, Z_μ) and the photon (A_μ) are not directly associated with the W_μ^α and B_μ fields, but are rather combinations of those fields.

The gauge symmetry is $\text{SU}_C(3) \times \text{SU}_L(2) \times \text{U}_Y(1)$. The first part, $\text{SU}_C(3)$, is the invariance under colour mixing of QCD described in the previous section. The $\text{SU}_L(2) \times \text{U}_Y(1)$ part is the gauge symmetry of the fields of the electroweak part of the Standard Model, which is not as easy to explain as QCD and is not described here in more detail.

The Lagrangian density of the Standard Model is defined by using the same assumptions that were described previously: Lorentz invariance, gauge symmetry and renormalisability. Predictions made with it have been shown to agree extremely well with data [12]. Interestingly, it is widely accepted that the Standard Model is only a very good approximation of a more fundamental but still unknown theory. To date, only one prediction of the Standard Model, the masslessness of the neutrinos, seems to be wrong, if not counting the Higgs boson that has still not been observed⁶, but these are not the only, often not even the primary, reasons that push people to look for a more fundamental theory. Deeper reasons include finding a theory with less free parameters than the Standard Model, trying to bridge the gap between gravity and the three other fundamental interactions and providing answers to some mysteries of cosmology.

That being said, whatever is the more fundamental theory, the Standard model remains a very, very good approximation of it at the energies currently involved in nuclear collisions in particle accelerators. The fact that there is physics beyond the Standard Model is, or at least is assumed to be, of no

⁵ Λ_{QCD} is defined differently at higher order. See [11, Section II-D-2].

⁶The search for the Higgs boson is underway at CERN's Large Hadron Collider (LHC).

importance for the present work.

2.2 From theory to experiments

It is in general non-trivial to extract experimentally measurable quantities from the Standard Model, and this is especially true if the strong interaction is involved. Two methods for calculating cross-sections are described in this section. The first is the S-matrix formalism, which allows to calculate cross-sections of *elementary particles* of the Standard Model. It is especially well suited for perturbative techniques and it works very well for the electroweak part of the model.

The second method is perturbative QCD (pQCD) and it used, as its name suggests, to calculate cross-sections for processes involving the strong interaction. Such calculations cannot be made with the S-matrix formalism because it is not cross-sections of quarks and gluons that are measured in particle accelerators, it is cross-sections of hadrons and nuclei, which are *bound states* of quarks and gluons (free quarks and gluons have *never* been encountered alone). Perturbative QCD addresses this problem with the idea of factorisation, which states that although some cross-sections cannot be completely calculated using perturbative techniques, the non-perturbative parts can be isolated and can be shown to be the same for different processes. This means that although pQCD cannot generally make predictions, it can give relations between the cross-sections of various processes. Another way of seeing this is that once the non-perturbative parts are fixed in experiments, they can be used to calculate other cross-sections.

Perturbative QCD is only useful if at least a part of the cross-section of a process is indeed perturbatively calculable. Asymptotic freedom suggests that the coupling constant of QCD is small only at high enough energies; the applicability of pQCD is limited to those high-energy processes. Other techniques have been developed to extract information, often observables other than cross-sections, from QCD when perturbative techniques cannot be used. The main ones are lattice QCD, effective Lagrangians and AdS/CFT. They are not described here as only cross-sections calculable with pQCD are studied in this thesis.

2.2.1 S-matrix formalism

The S-matrix formalism is a way to calculate, among other things, cross-sections and decay rates of elementary particles described by a quantum field theory, given the Lagrangian density of that theory. The argumentation that leads from the Lagrangian density to the final formulae involves some subtleties and is not explained here. The final formulae are rather simple, though. The formula for the cross-section, the only one needed here, is [6, Chapter 3]

$$d\sigma(\alpha \rightarrow \beta) = \frac{|\mathcal{M}_{\beta\alpha}|^2 (2\pi)^4}{4\sqrt{(p_1 \cdot p_2)^2 - m_1^2 m_2^2}} \delta^4 \left((p_1 + p_2) - \left(\sum_{j=1}^n k_j \right) \right) \prod_{f \in \beta} \frac{d^3 k_f}{2E_f (2\pi)^3} \quad (2.3)$$

where

$$\mathcal{M}_{\beta\alpha} = \langle \beta | \mathcal{H}_I(x=0) | \alpha \rangle + \frac{(-i)^2}{2!} \int dx^4 \langle \beta | T [\mathcal{H}_I(x) \mathcal{H}_I(x=0)] | \alpha \rangle + \dots \quad (2.4)$$

The variables m_1 and m_2 are the masses of the two initial particles, represented by initial state $|\alpha\rangle$, and p_1 and p_2 are their four-momenta. The final state $|\beta\rangle$ consists of n particles of four-momenta k_1, \dots, k_n .

The operator $\mathcal{H}_I(x)$ is the interacting Hamiltonian density, the part of the Hamiltonian density that is responsible for the interaction. It is usually related to the interacting Lagrangian density by $\mathcal{H}_I(x) = -\mathcal{L}_I(x)$ or by a slightly more complicated expression if $\mathcal{H}_I(x)$ contains derivatives.

Equation 2.4 is especially suited for perturbative calculations. The Hamiltonian density $\mathcal{H}_I(x)$ contains a coupling constant, and if this coupling constant is small enough, calculating only the first few terms of **equation 2.4** can be expected to give a reasonably accurate approximation of $\mathcal{M}_{\beta\alpha}$ and thus of $d\sigma(\alpha \rightarrow \beta)$.

2.2.2 Perturbative QCD

The precursor of perturbative QCD was the parton model, which was briefly presented in the introduction. The parton model was based on general physics principles and on experimental observations, but not on QCD itself. The development of QCD allowed to better understand why some of the ideas introduced by the parton model seemed to work very well, and why other did not.

The basis of pQCD is the factorisation theorems [11, Section IV]. Those are

proofs, derived from QCD, that various cross-sections can indeed be separated in perturbative and calculable parts, and non-perturbative but universal parts. What is often called *the* factorisation theorem is the idea that perturbative and non-perturbative parts are separable, but there are actually many theorems because the proofs are not the same for every process.

The starting point of the factorisation theorems is that most cross-sections can be expressed as

$$d\sigma = d\sigma_{[0]} + \left(\frac{Q_0}{Q}\right) d\sigma_{[1]} + \left(\frac{Q_0}{Q}\right)^2 d\sigma_{[2]} + \dots \quad (2.5)$$

where Q is the energy “scale” of the process, which is related to the part of the calculation that is expected to be perturbatively calculable. The variable Q_0 is another energy scale in the process, which should be much smaller than Q by assumption. It can be Λ_{QCD} , for example, or the mass of a particle involved in the process, depending on the process under consideration. Most of the factorisation theorems are proved for $d\sigma_{[0]}$ only. The first term, $d\sigma_{[0]}$, is called the *leading twist* contribution and the higher terms suppressed by powers of Q_0/Q are called higher twist contributions.

Saying that $d\sigma_{[0]}$ is factorisable means that it can be separated in perturbative and non-perturbative parts. For example,

$$d\sigma_{[0]} = F_1 \otimes F_2 \otimes d\hat{\sigma} \quad (2.6)$$

where F_1 and F_2 are unknown functions and $d\hat{\sigma}$ is a perturbatively calculable expression. The F_i and $d\hat{\sigma}$ usually depend on some common variables and \otimes denotes possible integration over those variables.

By assumption, $d\hat{\sigma}$ is perturbatively calculable and as such can be expressed as an expansion in the effective coupling $\alpha_s(Q)$,

$$d\hat{\sigma} = d\hat{\sigma}^{(0)} + \alpha_s(Q)d\hat{\sigma}^{(1)} + \alpha_s^2(Q)d\hat{\sigma}^{(2)} + \dots \quad (2.7)$$

where Q again appears as the energy scale of the process.

If only $d\hat{\sigma}^{(0)}$ is calculated, the cross-section is said to be calculated at *leading order* (LO). If the $d\hat{\sigma}^{(1)}$ term is *also* included, it is said to be a *next-to-leading order* (NLO) calculation, and so on. It is also possible in some cases to sum a part of *every* $d\hat{\sigma}^{(n)}$ instead of calculating $d\hat{\sigma}$ one order at the time. This is called resummation and it is meant to include in the calculation of **equation 2.7** terms that are large even if they are suppressed by large powers of

$\alpha_s(Q)$ [13]. The terms summed at all order are usually logarithms that become large in certain kinematic limits. Resummation of the largest logarithm is called leading log resummation, the second largest logarithm a next-to-leading log resummation and so on. Since resummation includes terms at all order, it includes some but not all the terms of the fixed-order calculations. To make an improvement over the fixed-order calculations, it is necessary to combine fixed-order and resummed calculations. Joining together resummed and fixed-order expansions requires at least to identify and remove the terms that were included in both expansions [14].

It is clear that for $d\sigma$ (equation 2.5) to be approximated well by $d\sigma_{[0]}$ and for the $d\hat{\sigma}$ perturbative expansion (equation 2.7) to be reliable, the scale Q must be large. It is also clear that as long as the non-perturbative parts F_i are unknown, no prediction can be made. There are thus important restriction on the type of processes for which predictions can be made. In the next section, a complete example of how those restrictions can be dealt with is presented for the case of single-particle inclusive production in hadron-hadron collisions.

Single-particle inclusive production in hadron-hadron collisions

Single-particle inclusive production in hadron-hadron collisions is the cross-section for producing a given particle, a π^0 meson or a photon for example, in a hadron-hadron collision. It is a cross-section that can be proved to be factorisable into perturbative and non-perturbative parts [11, Section IV–C–2]. At leading twist, the formula is

$$E_h \frac{d^3\sigma}{dp_h^3} = \sum_{a,b,c} \int dx_a dx_b \frac{dz_c}{z_c} f_{a/A}(x_a, Q_{\text{fac}}) f_{b/B}(x_b, Q_{\text{fac}}) \left[E_c \frac{d^3\hat{\sigma}}{dk_c^3}(Q_{\text{ren}}) \right] D_{h/c}(z_c, Q_{\text{frag}}) \quad (2.8)$$

where $f_{a/A}(x, Q)$ and $D_{h/c}(z, Q)$ are the non-perturbative functions and $d^3\hat{\sigma}(Q)$ is a perturbatively calculable parton-parton cross-section. The non-perturbative functions $f_{a/A}(x, Q)$ and $D_{h/c}(z, Q)$ are unknown, but they also appear in the leading twist formula of many other cross-sections for which factorisation is proved, for example electron-hadron collisions (DIS), e^-e^+ annihilation and dilepton production in hadron-hadron collisions (Drell-Yan) [15, Section 7&8]. Only $f_{a/A}(x, Q)$ appears in the formulae for DIS and Drell-Yan, and only $D_{h/c}(z, Q)$ in the formula for e^-e^+ annihilation. This means that if DIS and Drell-Yan are used to fix $f_{a/A}(x, Q)$ and e^-e^+ annihilation for $D_{h/c}(z, Q)$, pre-

dictions can be made for single-particle inclusive cross-sections.

The functions $f_{a/A}(x, Q)$ and $D_{h/c}(z, Q)$ are called respectively the parton distribution function (p.d.f.) of hadron “A” and the fragmentation function (f.f.) for particle “h”. In the parton model, the p.d.f. is interpreted as the probability that a parton of type “a” has a momentum fraction x of the momentum of hadron “A”, and the f.f. is interpreted as the probability that a parton “c” fragments into a particle “h” having a fraction z of the parton’s momentum.

Parton distribution functions and fragmentation functions depend on two variables, x/z and Q . The Q dependence is actually computable perturbatively for any range of Q where the effective strong coupling constant $\alpha_s(Q)$ is small enough for perturbative calculations to be trustable. In that case, the Q evolution is governed by the DGLAP equation⁷, which is similar but not identical for parton distribution functions and fragmentation functions. For p.d.f.’s, it takes the form [16, Section 3]

$$\mu \frac{df_{a/A}(x, \mu)}{d\mu} = \sum_b \int_x^1 \frac{d\xi}{\xi} P_{a/b}(\xi, \alpha_s(\mu)) f_{b/A}(x/\xi, \mu) \quad (2.9)$$

where the kernel $P_{a/b}$ is computable perturbatively. The Q dependence is thus known and p.d.f.’s and f.f.’s only need to be fitted for the variable x/z .

The perturbative part of [equation 2.8](#) is $d\hat{\sigma}(Q)$. It is a parton-parton cross-section and can be calculated using the S-matrix formalism described in the previous section. The result is a power expansion of $d\hat{\sigma}(Q)$ of the form of [equation 2.7](#) due to the perturbative expansion of [equation 2.4](#). For single-particle inclusive cross-sections, $d\hat{\sigma}(Q)$ is known at leading order and next-to-leading order. Leading log and next-to-leading log resummations are also known. For all those approximations of $d\hat{\sigma}(Q)$ to be reliable, however, Q must be large. In the present case, Q is of the order of the transverse momentum of the produced particle, which means that low order approximations of $d\hat{\sigma}(Q)$ can only be expected to be reliable for large transverse momentum (hard) particle production. A large Q is also desirable to make sure that the leading twist approximation is reliable too.

Assuming that there is enough experimental data to fix both the p.d.f. for hadrons “A” and “B” and the f.f. for particle “h”, [equation 2.8](#) can thus be used to predict the inclusive production of hard hadron “h” in collisions

⁷Also known as Altarelli-Parisi equation in older publications.

of a hadron “A” with a hadron “B”. In the next chapter, equation 2.8 is compared to experimental data for both hard π^0 and photon production in proton-proton collisions.

Chapter 3

Hard π^0 and photon production in proton-proton collisions

The leading twist formula for single-particle inclusive cross-sections in hadron-hadron collisions is equation 2.8. To make predictions for proton-proton collisions, a proton parton distribution function ($f_{a/p}(x, Q)$) is required, as well as a fragmentation function for π^0 ($D_{\pi^0/c}(z, Q)$) or photons ($D_{\gamma/c}(z, Q)$). An approximation for the perturbative part, $E_c d^3\hat{\sigma}/dk_c^3$, is also necessary.

Proton parton distribution functions are widely available nowadays. They are the results of fits to many sets of experimental data. As they are fits, they differ by the assumed forms of the fits, the number of free parameters used and the assumptions made to constrain some of these parameters. They also differ by the data sets used to do the fitting.

Fitting parton distribution functions is a difficult task and without enough data, the p.d.f.'s can be poorly constrained. Another problem is that some processes are fairly insensitive to certain p.d.f., a good example being the very weak dependence of DIS on the gluon distribution. These limitations have led to the inclusion of an increasingly large number of data sets from many different processes. Although the reasons to do so are good, it renders difficult the task of making predictions as envisioned originally, that is measure the non-perturbative functions (p.d.f.'s and f.f.'s) in a given set of processes and use them to make predictions about *other* types of processes. This goal can actually be quite complicated to achieve as what constitutes “another type

of process” is not very clearly defined.¹ It is thus very important to choose carefully which p.d.f. to use for a given calculation. The same applies to fragmentation functions, which are fitted in a similar way.

Another aspect of p.d.f.’s and f.f.’s that must be treated with care is the renormalisation and factorisation scheme in which they are defined. The procedures of renormalisation, which aims at eliminating divergences from the calculations, and factorisation, which allows to separate the perturbative and non-perturbative parts of a calculation, are not uniquely defined. Until quite recently, p.d.f.’s and f.f.’s used either the “fixed flavour number” (FFN) or the “zero mass variable flavour number” (ZM-VFN) factorisation scheme. Both are good approximations in certain kinematic ranges, but it is often necessary to make calculations outside those domains of applicability. To remedy to this problem, a scheme that superseded both, the “general mass variable flavour number” (GM-VFN) scheme, was developed. The basis of this scheme is an extended proof [17] of the factorisation theorems of [15, 16] so that they can be used in cases when Q is *not* much larger than the mass of all the quarks.²

Despite its much wider applicability, the GM-VFN scheme is much more difficult to use than the ZM-VFN scheme and the latter is still widely used. Actually, it is not yet known how to calculate single-particle inclusive cross-sections with the GM-VFN scheme beyond leading order. The ZM-VFN scheme thus has to be used, and appropriate p.d.f.’s and f.f.’s must be used with it. In general, “appropriate” means p.d.f.’s and f.f.’s defined using the ZM-VFN scheme.³ Care must also be taken about the choice of renormalisation scheme used with the factorisation scheme. The one generally used with the ZM-VFN factorisation scheme is the common “modified minimal subtraction” (\overline{MS}) renormalisation scheme.

A final word of caution about p.d.f.’s and f.f.’s must be made regarding the *order* at which they are known. Because p.d.f.’s and f.f.’s are extracted using factorised formulae, just like [equation 2.8](#), for which the perturbative part is known only at a given perturbative order, they are defined only at that same

¹For example, most people would agree that DIS, e^-e^+ annihilation and Drell-Yan are different processes, but Drell-Yan and photon production, or jet and hadron production, are similar processes. What constitutes a “real” prediction is debatable.

²It should be noted that there is some freedom in the proof that makes possible the definition of different but equally valid implementations of the GM-VFN scheme. See [18, Section 3].

³It is pointed out in [18, Section 4] and in [19] that if the scale Q is much larger than the mass of the quarks, it is also correct to use p.d.f.’s and f.f.’s defined in the GM-VFN scheme.

perturbative order. The same applies for their scale evolution (equation 2.9 for p.d.f.'s). To calculate equation 2.8 at a given order, it is important to use p.d.f.'s and f.f.'s defined at the same order, or at a higher order [13, Section 2].

There is no simple expression for the x/z and Q dependence of modern p.d.f.'s and f.f.'s: the x or z dependence is a fit to data and the known Q dependence is highly non-trivial. Both p.d.f.'s and f.f.'s are generally available numerically through programs provided by the authors of the fits. Libraries that regroup many p.d.f.'s are also available, the most recent one being LHAPDF⁴.

The case being settled for p.d.f.'s and f.f.'s, the final piece needed to calculate hard particle cross-sections is an expression for the perturbative part, $E_c d^3 \hat{\sigma} / dk_c^3$. As mentioned previously, this part is not known exactly but approximations at leading order, next-to-leading order, leading log and next-to-leading log are known. The leading order approximation is fairly simple and it is possible to write a program to calculate cross-sections at that order in a reasonable amount of time. A similar undertaking for the next-to-leading order approximation would require more time than most people are willing to invest in such a project, but it is possible to use programs made available online by generous researchers. The next-to-leading order results in this thesis are calculated with such a program.

Although leading order cross-sections are generally not accurate enough to reproduce experimental results, they allow to introduce in a simple way many ideas that remain true at higher orders. The leading order cross-section is presented in the next section for both π^0 meson and photon production. The next-to-leading order results are presented after.

3.1 Leading order cross-section

According to the S-matrix formalism, the leading order parton-parton cross-section is

$$d\hat{\sigma}^{LO} = \frac{|\mathcal{M}^{LO}|^2}{4\sqrt{(p_a \cdot p_b)^2 - m_a^2 m_b^2}} (2\pi)^4 \delta^4((p_a + p_b) - (p_c + p_d)) \frac{d^3 p_c}{2E_c (2\pi)^3} \frac{d^3 p_d}{2E_d (2\pi)^3} \quad (3.1)$$

with

$$\mathcal{M}^{LO} = \langle q_c(p_c), q_d(p_d) | \mathcal{H}_I(x=0) | q_a(p_a), q_b(p_b) \rangle \quad (3.2)$$

⁴<http://projects.hepforge.org/lhapdf/>

The q_i , $i \in \{a, b, c, d\}$, represent partons with four-momenta p_i .

In the centre-of-mass frame, the coordinate axes can be chosen such that the four-momenta of the protons are $P_A = (\sqrt{s}/2)(1, 0, 0, 1)$ and $P_B = (\sqrt{s}/2)(1, 0, 0, -1)$, where \sqrt{s} is the centre-of-mass energy of the system [20, Appendix]. The mass of the proton is neglected. The four-momenta of partons a and b are thus $p_a = (x_a\sqrt{s}/2)(1, 0, 0, 1)$ and $p_b = (x_b\sqrt{s}/2)(1, 0, 0, -1)$ if the masses of the quarks are also neglected.⁵

The four-momentum p_c is noted $p_c = (E_c, p_T^c, 0, p_l^c)$. Using the rapidity $y_c = (1/2) \ln((E_c + p_l^c)/(E_c - p_l^c))$, p_c can be written $p_c = p_T^c(\cosh y_c, 1, 0, \sinh y_c)$ for massless quarks.

Assuming a spin and colour average over the partons q_i , the possible values for the factor $\langle |\mathcal{M}^{LO}|^2 \rangle_{\text{color,spin}}$ are listed in [20, Table I], modulo a factor $1/(16\pi\hat{s}^2)$. The results are expressed in terms of the parton Mandelstam variables $\hat{s} = (p_a + p_b)^2$, $\hat{t} = (p_a - p_c)^2$ and $\hat{u} = (p_b - p_c)^2$, which can be rewritten $\hat{s} = x_a x_b s$, $\hat{t} = -x_a p_T^c \sqrt{s} e^{-y_c}$ and $\hat{u} = -x_b p_T^c \sqrt{s} e^{y_c}$ using the above definitions for p_a , p_b and p_c .

The spin and colour average of $d\hat{\sigma}^{LO}$ is thus

$$d\bar{\sigma}^{LO} \equiv \frac{\langle |\mathcal{M}^{LO}|^2 \rangle_{\text{color,spin}}}{16\pi^2 x_a x_b s} \delta^4((p_a + p_b) - (p_c + p_d)) \frac{d^3 p_c}{E_c} \frac{d^3 p_d}{2E_d} \quad (3.3)$$

Using the identity $d^3 p/2E = d^4 p \delta(p^2)$, the integral over p_d can be done easily. Also, $\delta(p_d^2) = \delta((p_a + p_b - p_c)^2)$ is equal to $\delta(\hat{s} + \hat{t} + \hat{u})$ for massless quarks. The differential cross-section can thus be written

$$E_c \frac{d^3 \bar{\sigma}^{LO}}{dp_c^3} = \frac{\langle |\mathcal{M}^{LO}|^2 \rangle_{\text{color,spin}}}{16\pi^2 \hat{s}} \delta(\hat{s} + \hat{t} + \hat{u}) \quad (3.4)$$

which is exactly the expression that enters the factorised formula for hard particle cross-sections (equation 2.8).

If $q_1 = u$, $q_2 = d$, $q_3 = u$ and $q_4 = d$, for example,

$$E_c \frac{d^3 \bar{\sigma}^{LO}}{dp_c^3} = \frac{\hat{s}}{\pi} \left[\frac{\langle |\mathcal{M}^{LO}|^2 \rangle_{\text{color,spin}}}{16\pi\hat{s}^2} \right] \delta(\hat{s} + \hat{t} + \hat{u}) = \frac{\hat{s}}{\pi} \left[\left(\frac{\pi\alpha_s^2(Q)}{\hat{s}^2} \right) \frac{4\hat{s}^2 + \hat{u}^2}{9\hat{t}^2} \right] \delta(\hat{s} + \hat{t} + \hat{u})$$

If q_3 and q_4 are exchanged, \hat{u} and \hat{t} are exchanged in the bracket. Every other parton-parton cross-section can be determined by the same technique using [20, Table I]. Of course, the $|\mathcal{M}^{LO}|^2$ terms could also be computed.

⁵The assumption only matters for quarks as gluons are thought to be massless.

Details on the calculations are available in [21, Appendix] for example.

A wide choice of parton distribution functions is available. A fairly recent one that uses the ZM-VFN scheme, CTEQ6 [22], is used. As π^0 fragmentation function, KKP [23] is used, for technical reasons, although more recent f.f.'s ([24, 25]) are available. For photons, BFG [26] is used as fragmentation function.

Only three parameters remain in [equation 2.8](#), the three scales Q_{fac} , Q_{ren} and Q_{frag} . The factorisation theorem only says that these scales should be, in the present case, of the order of the transverse momentum of the produced particle. If [equation 2.8](#) was known exactly, this freedom in the choice of scales would not be a problem since [equation 2.8](#) would be totally invariant under that choice of scales. Unfortunately, [equation 2.8](#) is known only at finite order, at rather low finite order actually, and it does depend on the choice of scales. At leading order, that scale dependence can be expected to be significant.

In the present case, the scales are all taken to be equal to a constant, κ , times the transverse momentum of the hadron/photon: $Q_{\text{fac}} = Q_{\text{ren}} = Q_{\text{frag}} = \kappa p_T^h$. The variable κ is set to three values, $\{1/2, 1, 2\}$. Although such a choice is rather arbitrary, it is at least a common one [10, Section 9.2.3]. It is very important to understand, however, that varying κ is *not* an estimation of the uncertainty due to the scales; it gives at best a very rough idea of how much the results depend on the choice of scales.

The final result is

$$E_h \frac{d^3 \bar{\sigma}^{\text{LO}}}{dp_h^3} = \sum_{a,b,c} \int dx_a dx_b \frac{dz_c}{z_c} f_{a/p}(x_a, \kappa p_T^h) f_{b/p}(x_b, \kappa p_T^h) \left[E_c \frac{d^3 \bar{\sigma}^{\text{LO}}}{dp_c^3} \right] D_{h/c}(z_c, \kappa p_T^h) \quad (3.5)$$

where the sum is over the gluon and the ‘‘active’’ quarks and antiquarks. A quark is considered active if its mass is smaller than the scale Q .⁶

The results for π^0 and photons are presented below.

3.1.1 π^0

The parton distribution function CTEQ6L1 is a leading order one fitted using $\alpha_s(Q)$ at leading order with $\alpha_s(M_Z) = 0.130$ and the leading order DGLAP

⁶Though it is thought to be correct to sum a and b , the ‘‘initial state’’ partons, over the number of active flavours, the tradition (adopted here) of doing the same thing for c , which is a ‘‘final state’’ parton, is probably incorrect. See [18, Section 2.3] and [19, Section II].

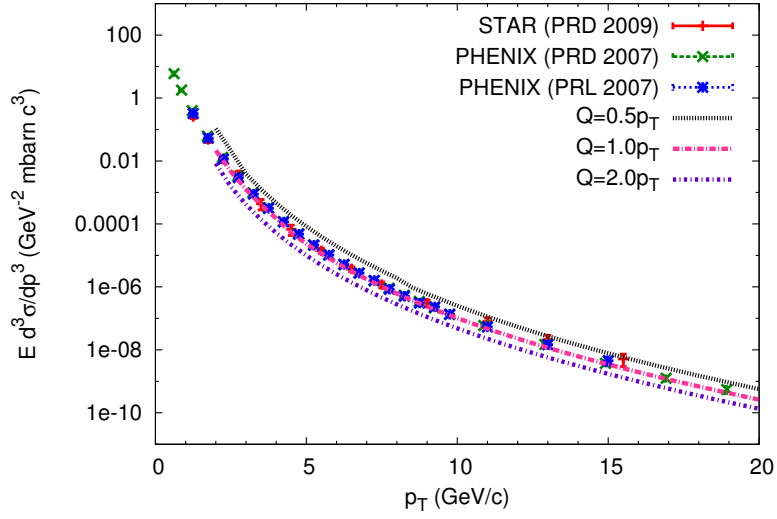


Figure 3.1: π^0 differential cross-section in proton-proton collisions at $\sqrt{s} = 200$ GeV and midrapidity compared to leading order calculations. $\alpha_s(M_Z) = 0.130$

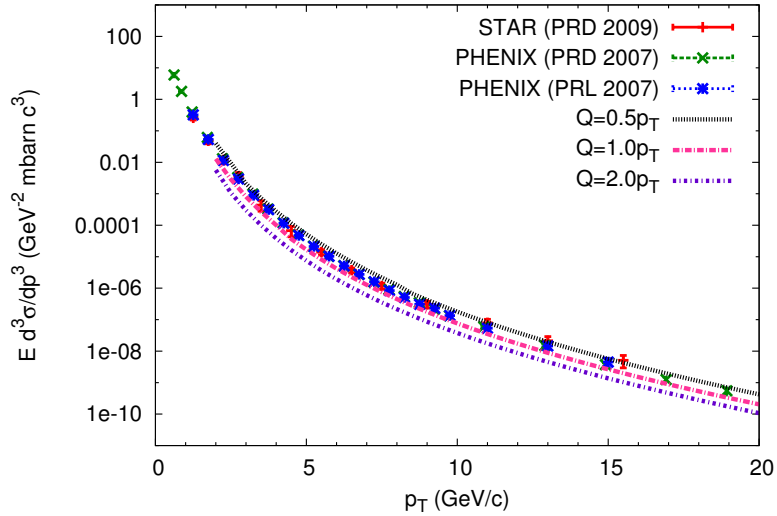


Figure 3.2: π^0 differential cross-section in proton-proton collisions at $\sqrt{s} = 200$ GeV and midrapidity compared to leading order calculations. $\alpha_s(M_Z) = 0.1181$

evolution equation [22, Section 3.1.3]. The leading order version of the fragmentation function KKP is used. It should be noted that $\alpha_s(M_Z)$ was considered to be a fitting parameter in KKP, and the value obtained at leading order is $\alpha_s(M_Z) = 0.1181$, which differs significantly from CTEQ6L1's value. As the choice $\alpha_s(M_Z)$ influences the calculations through $\alpha_s(Q)$, results are shown for both KKP's and CTEQ6L1's value.

At leading order, the formula for $\alpha_s(Q)$ can be written as

$$\alpha_s^{LO}(Q) = \left[2 \left(\frac{33 - 2n_A}{12\pi} \right) \ln \left(\frac{Q}{M_Z} \right) + \frac{1}{\alpha_s(M_Z)} \right]^{-1} \quad (3.6)$$

where n_A is the number of active flavours.

If $Q < m_c \approx 1.3 \text{ GeV}/c^2$, $n_A = 3$, if $m_c < Q < m_b \approx 4.2 \text{ GeV}/c^2$, $n_A = 4$ and if $Q > m_b$, $n_A = 5$.⁷

The differential cross-section $E_h d^3\sigma/dp_h^3$ is often rewritten using the rapidity y , the transverse momentum p_T and the azimuthal angle ϕ : $(1/p_T) d^3\sigma/dy d\phi dp_T$. In proton-proton collisions, an azimuthal symmetry is expected, so ϕ is usually integrated over: $1/(2\pi p_T) d^2\sigma/dy dp_T$.

Experimental data come from two detectors at RHIC, PHENIX [27, 28] and STAR [29]. All data were measured at a centre-of-mass energy of $\sqrt{s} = 200 \text{ GeV}$. Data from PHENIX cover a range of transverse momentum $p_T^{\pi^0}$ between 0.616 and 18.930 GeV/c and of pseudorapidity η of $|\eta| < 0.35$. Data from STAR cover $1.25 < p_T^{\pi^0} < 15.5 \text{ GeV}/c$ and $0 < \eta < 1$.

The differential cross-section $1/(2\pi p_T) d^2\sigma/dy dp_T$ is usually evaluated at a rapidity⁸ of $y = 0$ and for a range of p_T . This is what is done here.

Figures 3.1 and 3.2 shows the results for the two different values of $\alpha_s(M_Z)$. The error bars represent systematic and statistical errors added in quadrature.⁹

Both calculations are close to the data, especially in figure 3.1 where the curve for $Q = p_T^{\pi^0}$ is surprisingly good. It is clear, however, that the calculations depend significantly on the scales. This scale dependence is expected to be reduced at next-to-leading order.

⁷The sixth quark, the top one, is almost always ignored as its mass is very large ($m_t \approx 172 \text{ GeV}/c^2$).

⁸The rapidity y and pseudorapidity η are equal for a massless particle and approximately equal if the momentum of a particle is much larger than its mass. See [10, Section 39.5.2]. Since $m_{\pi^0} \approx 135 \text{ MeV}/c^2$, it is a good approximation to take $y \approx \eta$ for π^0 with energies higher than a few GeV/c .

⁹There is another type of experimental uncertainties: *normalisation* uncertainties. They are not shown on the figures.

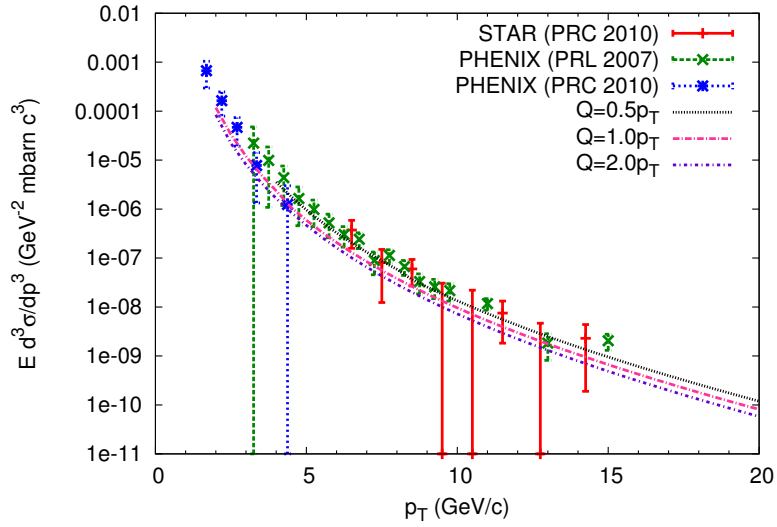


Figure 3.3: Photon differential cross-section in proton-proton collisions at $\sqrt{s} = 200$ GeV and midrapidity compared to leading order calculations. $\alpha_s(M_Z) = 0.130$

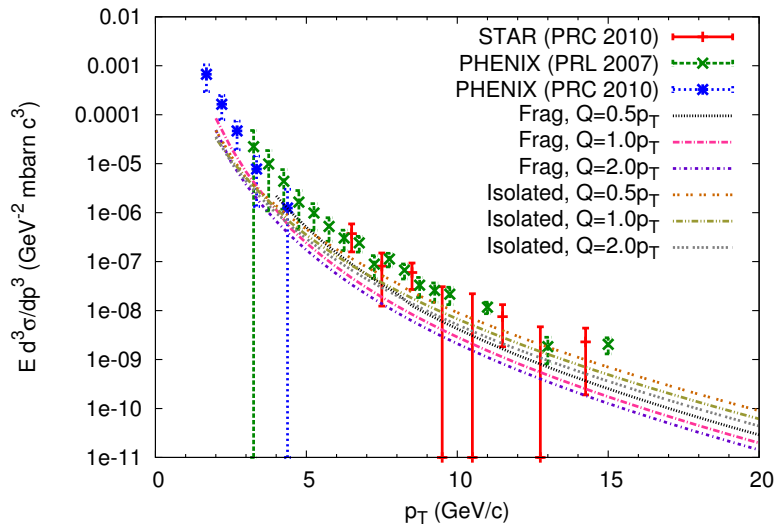


Figure 3.4: Separate fragmentation and isolated leading order calculations of photon differential cross-section in proton-proton collisions

3.1.2 Photons

Photon production in hadron-hadron collisions is different from hadron production because photons are elementary particles. As such, they can be produced directly in parton-parton collisions, without fragmentation, as well as through fragmentation. The former are called isolated photons, and the latter fragmentation photons.¹⁰ They are collectively known as prompt photons.

Fragmentation photons can be calculated using the same formula as for hadrons (equation 2.8) but with a parton-to-photon fragmentation function. Isolated photons can be calculated using equation 2.8 but with $\delta(z - 1)$ as fragmentation function and with different $E_c d^3\hat{\sigma}/dk_c^3$: instead of a parton in the final state, they have a photon. The $E_c d^3\hat{\sigma}/dk_c^3$ term is similar to equation 3.4 and the $|\mathcal{M}^{LO}|^2$ are also available in [20, Table I].

Again, CTEQ6L1 is used as leading order parton distribution function. The parton-to-photon fragmentation function used is BFG. It should be noted that BFG is a next-to-leading order fragmentation function, which is theoretically correct, although it is more common to use leading order p.d.f.'s and f.f.'s in leading order calculations.

Data are from PHENIX [31, 32] ($1.18 < p_T^\gamma < 4.37$ GeV/ c and $3.25 < p_T^\gamma < 15$ GeV/ c) and from STAR [33] ($6.5 < p_T^\gamma < 14.25$ GeV/ c), again at $\sqrt{s} = 200$ GeV.

The parameters are $\alpha_s(M_Z) = 0.130$ (CTEQ6L1's value) and $y = 0$. Set 2 of BFG is used. Figure 3.3 shows the sum of the isolated and fragmentation photon cross-sections, and figure 3.4 shows them separately. The agreement with the data of the sum of isolated and fragmentation photons is not as good as it was for π^0 : the calculations underestimate the data for most of the p_T^γ range. Again, the scale dependence is significant.

3.2 Next-to-leading order

As explained previously, a next-to-leading order calculation only means that the perturbative part of equation 2.8, $E_c d^3\hat{\sigma}/dk_c^3$, has to be computed at next-to-leading order. Appropriate p.d.f.'s and f.f.'s must also be used.

Calculating one extra order of $E_c d^3\hat{\sigma}/dk_c^3$ may seem to be a simple step but it is actually very complicated. The kinematics changes since states with

¹⁰There seems to be some confusion about the name that should be given to what are called here isolated photons. I chose to use the terminology from [30].

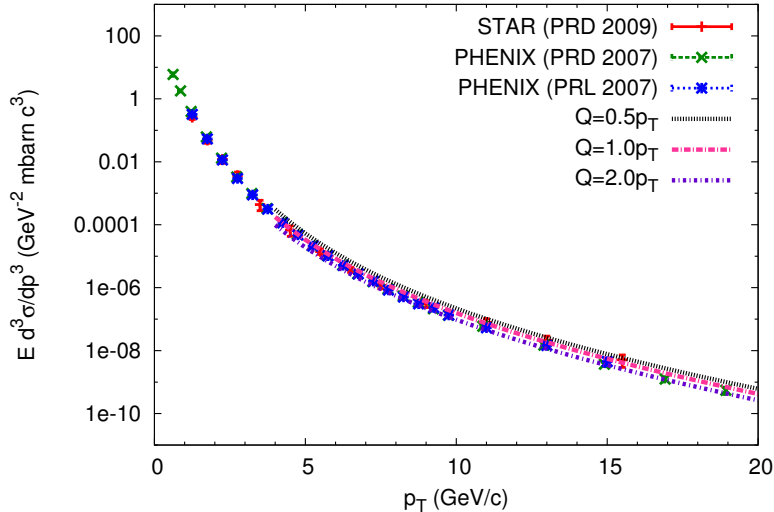


Figure 3.5: π^0 differential cross-section in proton-proton collisions at $\sqrt{s} = 200$ GeV and midrapidity compared to next-to-leading order calculations

three partons in the final state are now allowed, and divergences appear in some contributions to $|\mathcal{M}^{NLO}|^2$. Neither of these problems is insurmountable, but they do complicate the calculations significantly. Because of this, all next-to-leading order calculations in this thesis were made with INCNLO¹¹, the program of another research group. Although it is good to know how next-to-leading order calculations are made, it is not the main point here, and INCNLO allows to make such calculations with a limited understanding of the complicated matter of dealing with divergences.

The differential cross-section for photons, including isolated ones, and a variety of hadrons, including π^0 , can be calculated with INCNLO. It is based on [34] for isolated photon production at next-to-leading order and on [35] for fragmentation production. It should be noted that INCNLO uses a $\alpha_s(Q)$ with threshold matching¹², not the plain $\alpha_s(Q)$ formula like equation 3.6 that is discontinuous at every quark mass. Moreover, INCNLO is limited to $p_T^h \geq 4$ GeV/c. Finally, it can only calculate photon cross-sections with 4 active flavours ($n_A = 4$). Unless otherwise specified, next-to-leading order calculations are made with $n_A = 5$ for π^0 and $n_A = 4$ for photons.

A slightly modified version of CTEQ6M, CTEQ6.1M [37], is used as parton distribution function. It uses $\alpha_s(M_Z) = 0.118$. The next-to-leading order ver-

¹¹http://lappweb.in2p3.fr/lapth/PHOX_FAMILY/readme_inc.html

¹²Threshold matching is explained in [36] for example.

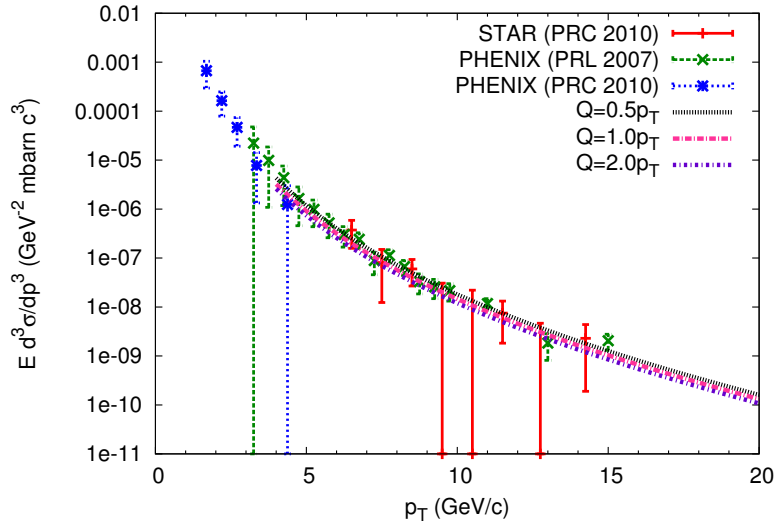


Figure 3.6: Photon differential cross-section in proton-proton collisions at $\sqrt{s} = 200$ GeV and midrapidity compared to next-to-leading order calculations

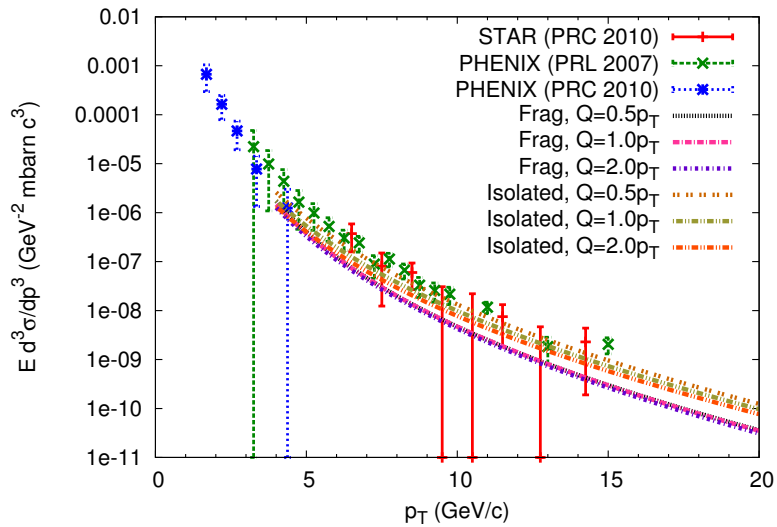


Figure 3.7: Photon differential cross-section in proton-proton collisions compared to separate isolated and fragmentation next-to-leading order calculations

sion of KKP, in which $\alpha_s(M_Z)$ was fitted to 0.1170, is used as π^0 fragmentation function. The photon fragmentation function is BFG again. It is not indicated in [26] what value of $\alpha_s(M_Z)$ was used in the fitting of BFG, only the value of $\Lambda_{\text{QCD}}^{(4)}$ is specified. Unfortunately, $\Lambda_{\text{QCD}}^{(n_A)}$ is not a uniquely defined quantity and it is not clear how to translate it into an $\alpha_s(M_Z)$ value in this case. For both π^0 and photons, the $\alpha_s(M_Z)$ of the p.d.f. was used for the calculations.

Figure 3.5 shows the next-to-leading order calculations for π^0 production compared with the same data that were shown with the leading order calculations. Figure 3.6 shows the same thing but for photons, the individual contribution to isolated and fragmentation photons being shown in figure 3.7. For both π^0 and photons, the calculations agree with the data rather well. The scale dependence is smaller than that of the leading order calculations, as expected.

Chapter 4

Hard π^0 and photon production in deuteron-gold collisions

In the previous chapter, it was shown that the leading twist, next-to-leading order formula for single-particle inclusive cross-sections in proton-proton collisions is in good agreement with data, despite a significant scale dependence of the calculations and the sometimes large uncertainties of the data. This good agreement indicates that production of hard particles like π^0 and photons in proton-proton collisions is well understood, and that makes hard π^0 and photons promising tools to study more complex processes like nucleus-nucleus collisions.

High-energy collisions of very large nuclei are enormously more complex than hadron-hadron collisions. On the other hand, hadron-nucleus collisions or collisions of nuclei in which no QGP is created are a more reasonable step toward understanding heavy ion collisions. Hard π^0 and photon data were collected at RHIC for deuteron-gold collisions, which are not quite hadron-nucleus collisions but almost since the deuteron is a very small nucleus. Equally importantly, no QGP is thought to be formed in deuteron-gold collisions.

It was already mentioned in the introduction that it is not known how to calculate with pQCD the single-particle inclusive cross-section for collisions like deuteron-gold ones, [equation 2.8](#) being only proved for collisions of hadrons. However, a *model* based on the concept of binary scaling was developed to bridge this gap between hadron-hadron collisions and nucleus-nucleus ones. This model is able to describe well cross-sections of hard particles in deuteron-gold collisions.

The Glauber model, the basis of the binary scaling hypothesis, is described

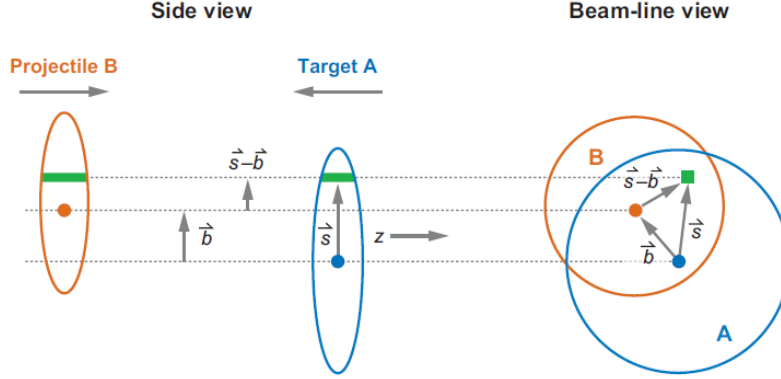


Figure 4.1: Geometry of a nucleus-nucleus collision. Figure from [38, Figure 3]

below. How it can be combined with pQCD to calculate cross-sections in deuteron-gold collisions is explained after.

4.1 Collisions according to the Glauber model

In the previous chapters, a formula was presented for the single-particle inclusive cross-sections in a hadron-hadron collision. What was meant by “hadron-hadron collisions” was really *inelastic* hadron-hadron collisions, as there is creation of particles. The formula must thus be compared with data from particle production in inelastic hadron-hadron collisions, as was done in the previous section (although it was not specified).

For collisions involving larger nuclei, a classification in elastic and inelastic collisions is not quite enough. Instead, a parameter \mathbf{b} is used to characterise the collisions, as shown in figure 4.1: \mathbf{b} is the vector going from the centre¹ of one nucleus, in the plane perpendicular to the collision axis (the “ z ” axis), to the centre of the other one. A large $b = |\mathbf{b}|$ means that the nuclei barely interact with each other, most likely an elastic collision or no collision at all, while a small b should mean an inelastic collision. Experimentally, it is not possible to determine the value of b at which a collision occurred, but it is possible to classify groups of collisions in ranges of b , called *centrality classes*. What is needed is thus a formula that gives a cross-section averaged over a range of parameter b . This is a quantity calculable in the Glauber model.

What is called the Glauber model in high-energy physics is a very simplified form of a “quantum theory of collisions of composite objects” [38, Section 2.1].

¹The nuclei are assumed to be spherically symmetric since the “centre” is only well-defined in that case, the orientation of the nuclei not being known.

It is used in two incarnations, the optical Glauber model and the Monte Carlo Glauber model. The latter is more precise but purely numerical, while the former can be expressed in an analytical form. The optical Glauber model is easier to explain and to use, and it is the one used in this thesis.

In the optical Glauber model, the differential inelastic cross-section of a nucleus-nucleus collisions is [38, Section 2.3]

$$d^2\sigma_{\text{inel}}^{AB} = d^2b \left[1 - \left(1 - \sigma_{\text{inel}}^{NN} \hat{T}_{AB}(b) \right)^{AB} \right] \quad (4.1)$$

where

$$\hat{T}_{AB}(\mathbf{b}) = \int d^2s \hat{T}_A(\mathbf{b}) \hat{T}_B(\mathbf{s} - \mathbf{b}) \quad (4.2)$$

and

$$\hat{T}_A(\mathbf{s}) = \frac{1}{A} \int dz_A \rho_A(\mathbf{s}, z_A) \quad (4.3)$$

The function $\rho_A(\mathbf{s}, z_A)$ represents the nucleon density of nucleus A and $\sigma_{\text{inel}}^{NN}$ is the nucleon-nucleon inelastic cross-section, which is assumed to be the same for every type of nucleon-nucleon collisions (proton-proton, proton-neutron, neutron-neutron). The number of nucleons in each nucleus is denoted by A and B , \mathbf{b} was described previously and the geometrical interpretation of \mathbf{s} is shown in figure 4.1.

Taking the derivative of $d^2\sigma_{\text{inel}}^{AB}$ yields

$$E \frac{d^5\sigma_{\text{inel}}^{AB}}{dp^3} = d^2bAB \left(E \frac{d^3\sigma_{\text{inel}}^{NN}}{dp^3} \right) \hat{T}_{AB}(b) \left[1 - \left(E \frac{d^3\sigma_{\text{inel}}^{NN}}{dp^3} \right) \hat{T}_{AB}(b) \right]^{AB-1} \quad (4.4)$$

Equation 4.4 can be simplified by expanding the brackets in a Taylor series:

$$E \frac{d^5\sigma_{\text{inel}}^{AB}}{dp^3} = d^2bAB \left(E \frac{d^3\sigma_{\text{inel}}^{NN}}{dp^3} \right) \hat{T}_{AB}(b) \left[\sum_{n=0}^{\infty} \binom{AB-1}{n} \left(- \left(E \frac{d^3\sigma_{\text{inel}}^{NN}}{dp^3} \right) \hat{T}_{AB}(b) \right)^n \right] \quad (4.5)$$

If $(E d^3\sigma_{\text{inel}}^{NN}/dp^3) \hat{T}_{AB}(b) \ll 1$, it is possible to keep only the first term in the brackets, 1:

$$E \frac{d^5\sigma_{\text{inel}}^{AB}}{dp^3} = d^2bAB \left(E \frac{d^3\sigma_{\text{inel}}^{NN}}{dp^3} \right) \hat{T}_{AB}(b) \quad (4.6)$$

On the other hand, also according to the optical Glauber model, the number

of binary nucleon collisions in the nucleus-nucleus collision is [38, Section 2.3]

$$N_{\text{binary}}(b) = AB\hat{T}_{AB}(b)\sigma_{\text{inel}}^{NN} \quad (4.7)$$

Thus,

$$E\frac{d^5\sigma_{\text{inel}}^{AB}}{dp^3} = d^2b\left(E\frac{d^3\sigma_{\text{inel}}^{NN}}{dp^3}\right)\frac{N_{\text{binary}}(b)}{\sigma_{\text{inel}}^{NN}} \quad (4.8)$$

Equation 4.8 is not especially useful computationally since it is $\hat{T}_{AB}(b)$ that is known in the optical model, not $N_{\text{binary}}(b)$, but it allows to express $E d^3\sigma_{\text{inel}}^{AB}/dp^3$ in terms of easily understandable quantities: the differential ($E d^3\sigma_{\text{inel}}^{NN}/dp^3$) and total ($\sigma_{\text{inel}}^{NN}$) inelastic nucleon-nucleon cross-section and the number of binary collisions for a given value of b .

The differential cross-section $E d^3\sigma_{\text{inel}}^{AB}/dp^3$ can be found by integrating over the appropriate range of b , depending on the centrality class wanted. If there is no centrality class selection, what is called *minimum bias* (MB), b must be integrated over all space and the formula simplifies to

$$\left\langle E\frac{d^3\sigma_{\text{inel}}^{AB}}{dp^3} \right\rangle_{\text{MB}} = \left(E\frac{d^3\sigma_{\text{inel}}^{NN}}{dp^3} \right) AB \quad (4.9)$$

It should be remembered that all those quantities are defined in the optical Glauber model, which is an approximation of the Glauber model. The approximation is expected to be good for large A and B and small $\sigma_{\text{inel}}^{NN}$ (or $d\sigma_{\text{inel}}^{NN}$) [38, Section 2.5].

4.1.1 Binary scaling

As was seen in the previous section, it is not the measured quantity $\langle E d^3\sigma_{\text{inel}}^{AB}/dp^3 \rangle$ that scales as the number of binary collisions, it is the differential, unmeasured **equation 4.8**. In particular, the common quantity $\langle E d^3\sigma_{\text{inel}}^{AB}/dp^3 \rangle_{\text{MB}}$ scales with AB . All this is according to the approximative optical Glauber model.

Faith in the validity of **equation 4.9** comes largely from various experimental confirmations. For example, figure 4.2, taken from [39], shows that the Drell-Yan cross-section in various proton-nucleus collisions scales with A , the number of nucleons in the nucleus. Actually, a correction to **equation 4.9** is already introduced in that paper, an isospin correction. The aim is to correct for the assumption that $\sigma_{\text{inel}}^{NN}$ is the same for every nucleon-nucleon collision, an assumption that is only approximative. As can be seen in figure 4.2, the isospin-corrected scaling is quite good.

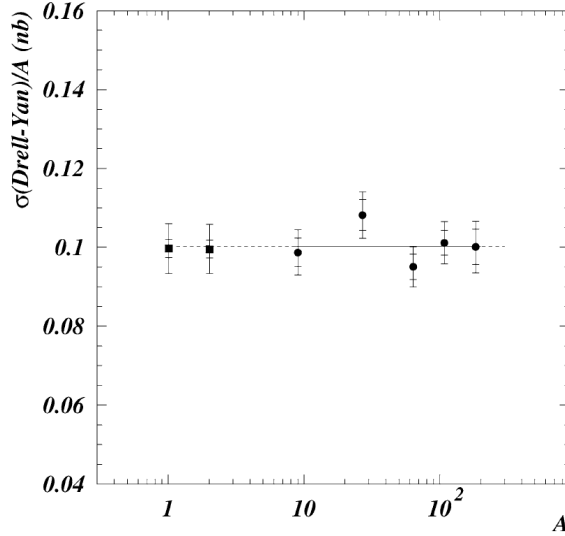


Figure 4.2: Scaling with A of the isospin-corrected Drell-Yan cross-section for various proton-nucleus collisions. Figure from [39, Figure 3]

It is comparisons like this one that have made “binary scaling” such a well accepted idea. It never works quite perfectly, but with “reasonable” modifications it can reproduce well a wide range of observations. It is important to remember, however, that even if they do seem to work quite well, formulae like [equation 4.9](#) are in no way as well established as e.g. the formulae presented in the previous chapters based on the factorisation theorems.

4.2 Deuteron-gold collisions and nuclear effects

[Equation 4.9](#) is the starting point for calculating hard π^0 and photon production in deuteron-gold collisions. It is a very simple formula whose only inputs are the number of nucleons and a proton-proton cross-section. With [equation 2.8](#) as formula for the proton-proton cross-section, [equation 4.9](#) is in full

$$\begin{aligned}
 \left\langle E_h \frac{d^3\sigma_{\text{inel}}^{AB}}{dp_h^3} \right\rangle_{\text{MB}} &= AB \sum_{a,b,c} \int dx_a dx_b \frac{dz_c}{z_c} f_{a/A}(x_a, Q_{\text{fac}}) f_{b/B}(x_b, Q_{\text{fac}}) \\
 &\quad \times \left[E_c \frac{d^3\hat{\sigma}}{dk_c^3}(Q_{\text{ren}}) \right] D_{h/c}(z_c, Q_{\text{frag}}) \quad (4.10)
 \end{aligned}$$

Figures 4.3 and 4.4 shows a comparison of [equation 4.10](#), calculated at next-to-leading order, with data. The parameters used for the calculations

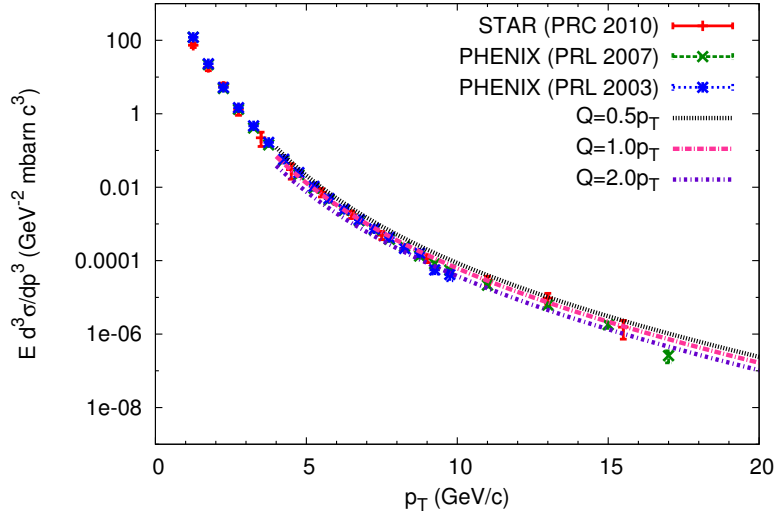


Figure 4.3: π^0 differential cross-section in minimum bias deuteron-gold collisions at $\sqrt{s_{NN}} = 200$ GeV and midrapidity compared to scaled proton-proton calculations

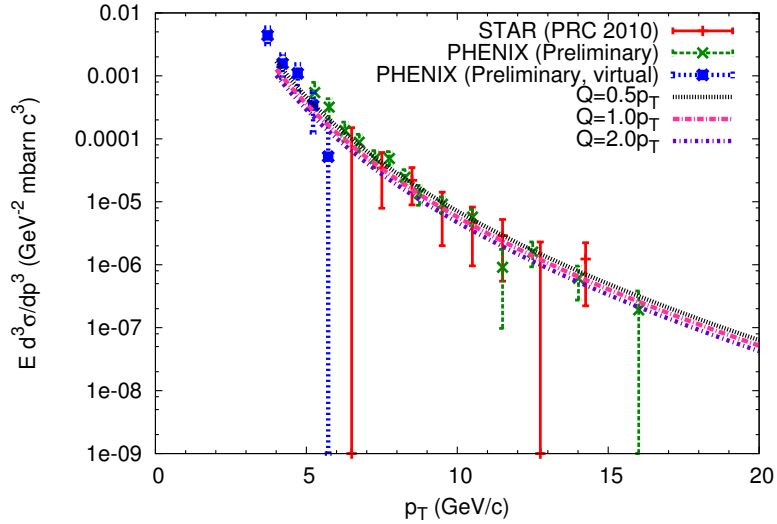


Figure 4.4: Photon differential cross-section in minimum bias deuteron-gold collisions at $\sqrt{s_{NN}} = 200$ GeV and midrapidity compared to scaled proton-proton calculations

are the same as in section 3.2. Data² for hard π^0 production in deuteron-gold collisions come from STAR [33] and PHENIX [28, 40]. Data for photon production come from the same paper from STAR, and there are also preliminary data from PHENIX [41]. A further set of preliminary data from PHENIX [44], extracted using the dilepton (virtual photon) yield as in [31], is included. All data are at $\sqrt{s_{NN}} = 200$ GeV, which means that the centre-of-mass energy *per nucleon* is 200 GeV.

The π^0 data are well described by [equation 4.10](#). The calculations seems to underestimate the photon data, especially at low p_T^γ , but definitive conclusions are difficult to draw due to the much larger uncertainties on the data.

Comparisons with the cross-sections are not the best way to study the agreement of [equation 4.10](#) with data. It is possible to study another quantity that provides similar information as figures 4.3 and 4.4. This quantity is the nuclear modification factor.

4.2.1 Nuclear modification factor and the isospin effect

For minimum bias collisions, the nuclear modification factor is defined as

$$\langle R_{AB} \rangle_{\text{MB}} = \frac{\left\langle E \frac{d^3 \sigma_{\text{inel}}^{AB}}{dp^3} \right\rangle_{\text{MB}}}{AB \left(E \frac{d^3 \sigma_{\text{inel}}^{PP}}{dp^3} \right)} \quad (4.11)$$

If the numerator is taken to be equal to [equation 4.10](#), the calculated value of [equation 4.11](#) is 1, assuming that both the numerator and the denominator are calculated with the same parameters (p.d.f., f.f., $\alpha_s(M_Z)$, scales, ...). As such, a plot of $\langle R_{AB} \rangle_{\text{MB}}$ with experimental values provides similar information as figures 4.3 and 4.4, that is, whether or not nucleus-nucleus collisions are equivalent to binary scaled proton-proton collisions.

Data for $\langle R_{AB} \rangle_{\text{MB}}$ are presented in figures 4.5 and 4.6. As it can be seen, both STAR data for π^0 [33] and preliminary PHENIX data for photons [41] have very large uncertainties and are of limited use. On the other hand,

²Data from [40] and [41] are not presented as cross-sections but rather as a quantity called the yield, generally noted N . For minimum bias data, the yield is related to the cross-section by

$$d^3 N_{AB} = \frac{1}{\sigma_{\text{inel}}^{AB}} d^3 \sigma_{AB}$$

where $\sigma_{\text{inel}}^{AB}$ is the total inelastic cross-section of the collision [42]. Here, the value of $\sigma_{\text{inel}}^{dAu}$ used to translate yields in cross-sections is 2.26 barn [28, 43].

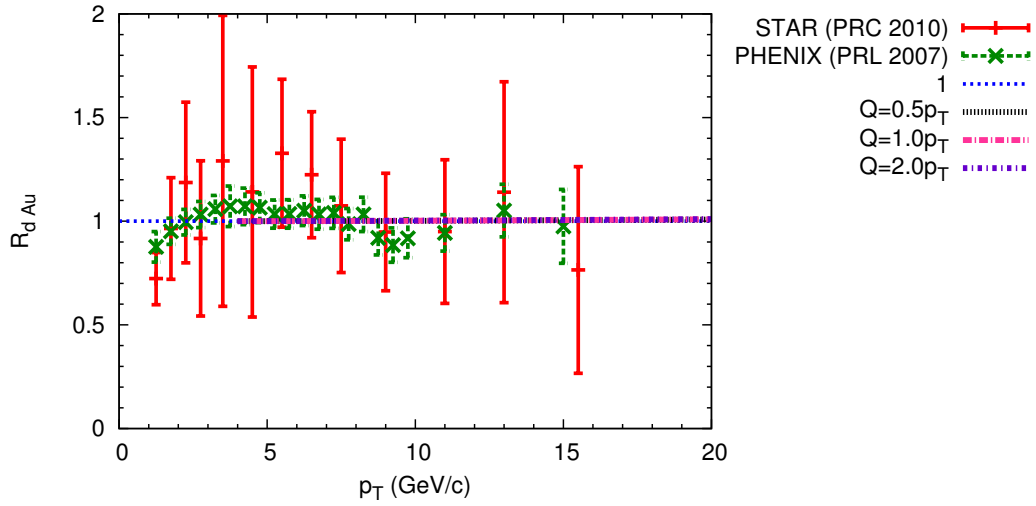


Figure 4.5: $\langle R_{dAu} \rangle_{MB}$ for π^0 compared to isospin-corrected calculations

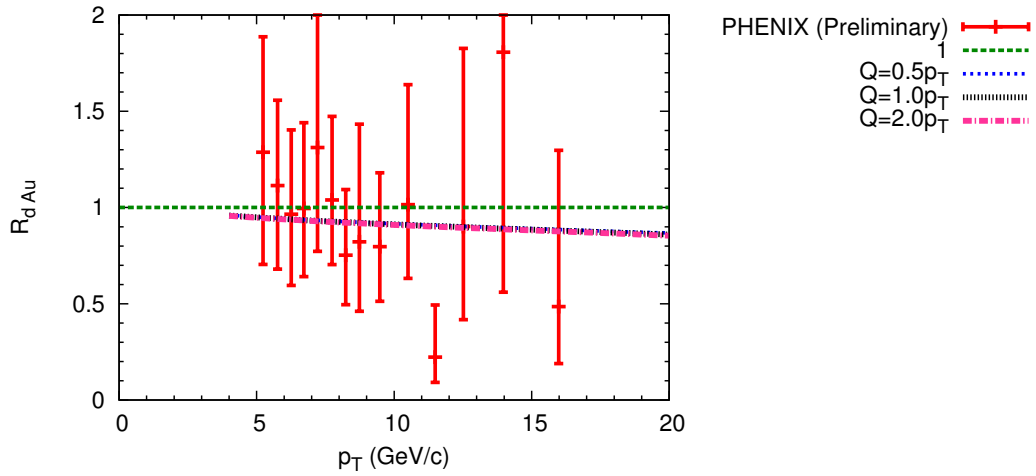


Figure 4.6: $\langle R_{dAu} \rangle_{MB}$ for photons compared to isospin-corrected calculations

PHENIX data for π^0 [28] have smaller uncertainties and can be expected to provide some constraints on necessary modifications to [equation 4.10](#). For this reason, what follows will be focused on π^0 , although photon data and calculations will still be presented.

Data in [figure 4.5](#) suggests that the measured $\langle R_{AB} \rangle_{\text{MB}}$ is slightly larger than 1 (enhancement) in the lower range of $p_T^{\pi^0}$ but decreases below 1 (suppression) around $p_T^{\pi^0} \approx 9$ GeV/ c . The last data points, which shows a possible increasing trend, are ignored due to the larger uncertainties and the small number of points. The apparent suppression in the first data points is also ignored as it is in a range where the reliability of pQCD calculations is expected to be questionable. The hypothesis investigated is that the enhancement in the $p_T^{\pi^0} \approx 4$ to 9 GeV/ c range and the subsequent suppression above 9 GeV/ c is caused by nuclear effects.

A first correction to [equation 4.10](#) that should be expected is the isospin effect, which was mentioned in the previous section. The isospin effect is not really a nuclear effect, it is only a correction for the incorrect assumption that all nucleon-nucleon collisions have the same cross-section.

It is possible to correct that assumption, at least in part, in a simple manner by defining an isospin-averaged p.d.f.:

$$\bar{f}_{a/A}(x, Q) = \frac{Z}{A} f_{a/p}(x, Q) + \frac{A-Z}{A} f_{a/n}(x, Q) \quad (4.12)$$

where A is the number of nucleons, Z is the charge of nucleus A , $f_{a/p}(x, Q)$ is a proton p.d.f. and $f_{a/n}(x, Q)$ a neutron one.

Neutron p.d.f.'s are related to proton ones by the isospin symmetry, an approximative but quite good symmetry [6, Section 9.2.3]. According to that symmetry, the relations between neutron and proton p.d.f.'s are

$$\begin{aligned} f_{u/n}(x, Q) &= f_{d/p}(x, Q); & f_{d/n}(x, Q) &= f_{u/p}(x, Q) \\ f_{\bar{u}/n}(x, Q) &= f_{\bar{d}/p}(x, Q); & f_{\bar{d}/n}(x, Q) &= f_{\bar{u}/p}(x, Q) \\ f_{a/n}(x, Q) &= f_{a/p}(x, Q) \text{ for all other partons} \end{aligned} \quad (4.13)$$

Using $\bar{f}_{a/A}(x, Q)$ to calculate [equation 4.10](#) in [equation 4.11](#) results in the curves shown in [figures 4.5](#) and [4.6](#). It can be seen that the isospin effect decreases the photon cross-section notably. The effect on π^0 is insignificant, the curves being almost equal to 1 for the whole range of $p_T^{\pi^0}$. This is in part due to the fact that the quark content of π^0 is isospin invariant.

Thus, although the isospin effect is a required modification to [equation 4.10](#),

it does not improve the agreement of the calculations with data. Figures 4.5 and 4.6 show something very interesting about the calculations however: the scale dependence of calculations using [equation 4.11](#) seems to be significantly reduced with respect to that of calculated cross-sections like those shown in figures 4.3 and 4.4. This much smaller scale dependence is a very interesting characteristic of $\langle R_{AB} \rangle$, but it deserves some explanations.

The formula used to calculate the numerator of [equation 4.11](#) is [equation 4.10](#) with isospin-corrected p.d.f.'s. As [equation 4.10](#) is based on the proton-proton cross-section formula, which is the denominator of [equation 4.11](#), the fact that the scale dependence seems to largely cancel is somewhat understandable, though not obvious. In the rest of this chapter and in the following one, further modifications will be made to the formula for the deuteron-gold cross-section but it will be seen that the scale dependence of $\langle R_{dAu} \rangle$ remains very small, a fact that is again not obvious from a theoretical point of view remembering that the scale dependence of the formulae for the cross-sections is rather complicated. It is not clear if this small scale dependence of $\langle R_{dAu} \rangle$ is real or is an artifact of the specific choice of formula used for the deuteron-gold cross-section: the possibility that the scale dependence is merely underestimated and not actually reduced cannot be ruled out.

Another choice that may hide the real scale dependence is the use of the same scales in both the numerator and the denominator; that is, the scales that enter the cross-sections are varied by factors of two *simultaneously* in the numerator and the denominator. It is not clear if this is correct or if they should be varied independently, which would likely result in an increased scale dependence. This warning and the previous one about the reliability of the estimate of the scale dependence of $\langle R_{dAu} \rangle$ must be kept in mind when it is said that the scale dependence is small and in particular smaller than that of the cross-section calculations.

It is now necessary to turn to other sources of nuclear effects to see if agreement with data can be improved.

4.2.2 Nuclear parton distribution functions

Even with the isospin effect taken into account, [equation 4.10](#) remains a very simple formula for explaining hard particle production in deuteron-gold collisions, a process that is, after all, not that simple with respect to hadron-hadron collisions. As was seen in figures 4.5 and 4.6, it is difficult to tell from

the current data if hard π^0 and photon production in deuteron-gold collisions can really be explained well by isospin-corrected binary scaling alone. There are some indications from $p_T^{\pi^0}$ data, however, that this is not the case.

There are a number of proposed sources of nuclear effects. Many are explained in [45], a comprehensive review on the subject. Here, instead of trying to take into account nuclear effects with various theoretical models, a phenomenological approach is taken. Nuclear effects are assumed to be absorbed in *nuclear parton distribution functions*, the equivalent of proton parton distribution functions for nuclei. To understand what are nuclear p.d.f.'s and what kinds of nuclear effects they take into account, it is necessary to understand how they are defined.

The core assumption in the definition of nuclear p.d.f.'s is that the factorisation theorems also apply, at least to a good approximation, to processes involving nuclei. That is, it is assumed that the formulae for the cross-section of processes like nuclear deep-inelastic scattering, or Drell-Yan or hard particle production in nucleus-nucleus collisions can also be expressed as the convolution of parton distribution functions, a perturbative part and in some cases a fragmentation function. The fragmentation function is usually assumed to be the same as for hadron-hadron collisions, but the p.d.f. is now a *nuclear* parton distribution function. Binary scaling is also assumed and the isospin effect is generally included too.

According to those assumptions, the minimum bias single-particle inclusive cross-sections for a nucleus-nucleus collisions is thus *defined* as

$$E_h \frac{d^3 \sigma_{AB}^{\text{inel}}}{dp_h^3} = AB \sum_{a,b,c} \int dx_a dx_b \frac{dz_c}{z_c} F_{a/A}(x_a, Q_{\text{fac}}) F_{b/B}(x_b, Q_{\text{fac}}) \times \left[E_c \frac{d^3 \hat{\sigma}}{dk_c^3}(Q_{\text{ren}}) \right] D_{h/c}(z_c, Q_{\text{frag}}) \quad (4.14)$$

where $F_{a/A}(x, Q)$ is the nuclear p.d.f. for a nucleus A . As nuclear p.d.f.'s are assumed to be universal just as hadron p.d.f., they can be measured in other processes like electron-nucleus collisions and Drell-Yan in nucleus-nucleus collisions. Various parametrisation of nuclear p.d.f. are available, EKS98 [46], nDS [47], HKN07 [48] and EPS09 [49] being recent ones.

Equation 4.14 is appealing as it includes binary scaling and the isospin effect, but also promises to include all other significant nuclear effects into the nuclear parton distribution function. It is important to remember, however,

that some of the assumptions that led to [equation 4.14](#) are debatable. The universality of the nuclear p.d.f.'s is not proven, only assumed, and it is not clear that all nuclear effects, which have very different origins, can really be taken into account by nuclear p.d.f.'s.

The assumption that nuclear p.d.f.'s are universal is actually testable to some extent: the data used to define nuclear p.d.f.'s are from different processes, and if the data can be fitted well assuming factorisation in collisions involving nuclei, it is an indication that assuming factorisation may be at least a good approximation. Also, if some nuclear effects are significant and really cannot be included in the nuclear p.d.f., it should lead to problems in the fitting process. Of course, what is a good fit is also debatable. Another method of assessing the universality of nuclear p.d.f.'s has been proposed in [50].

It is clear that the “nuclear p.d.f. approach” comes with great promises but potentially very serious flaws. These possible weaknesses are not investigated in this thesis; the nuclear p.d.f. approach is used and assumed to be usable for the rest of this work. Results are presented in the next section.

4.3 Comparison with data

Calculating [equation 4.11](#) with [equation 4.14](#) as numerator is fairly straightforward. The parameters are fixed the same way as in [section 3.2](#): $Q_{\text{fac}} = Q_{\text{ren}} = Q_{\text{frag}} = \kappa p_T^h$ ($\kappa \in \{1/2, 1, 2\}$), $y = 0$, $\sqrt{s_{NN}} = 200$ GeV, KKP-NLO is used as π^0 fragmentation function, BGF-2 as photon fragmentation function and $\alpha_s(M_Z)$ is taken to be the value used in the parametrisation of the nuclear p.d.f.

Two different nuclear p.d.f.'s are used, HKN07 and EPS09. Both are available at leading order and next-to-leading order, but are used at NLO. The older EKS98 is not used as it is only available at LO. It has not been possible to use nDS for technical reasons. It should be noted that EPS09 used as data sets hard π^0 data from deuteron-gold collisions at RHIC — the very data with which the present calculations of $\langle R_{dAu}^{\pi^0} \rangle_{\text{MB}}$ are compared with. However, as [figure 4.7](#) shows, $\langle R_{dAu}^{\pi^0} \rangle_{\text{MB}}$ calculated at leading order with EPS09 and EKS98 are almost identical. Since EKS98 did not use any RHIC data as data set, it indicates that the inclusion of π^0 data from RHIC in EPS09 does not affect significantly the calculation of $\langle R_{dAu}^{\pi^0} \rangle_{\text{MB}}$. This is a rather surprising conclusion, but a very fortunate one as EPS09 would have been unusable if it had been

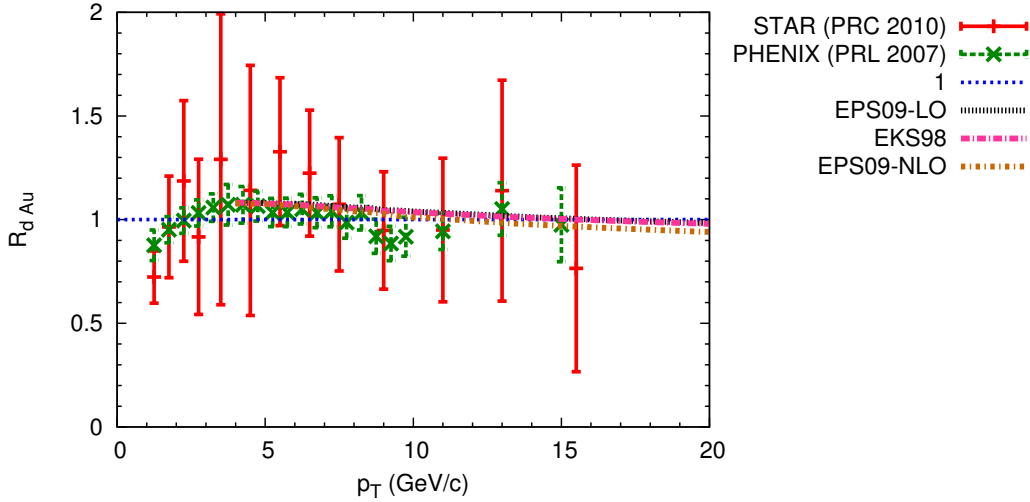


Figure 4.7: $\langle R_{dAu} \rangle_{\text{MB}}$ for π^0 compared to leading order calculations with EKS98 and EPS09 (LO nuclear p.d.f., f.f., $\alpha_s(Q)$, ...) and next-to-leading order calculation with EPS09 (NLO nuclear p.d.f., f.f., $\alpha_s(Q)$, ...). $Q_{\text{fac}} = Q_{\text{ren}} = Q_{\text{frag}} = p_T^{\pi^0}$

significantly biased. It has been verified that the same is true for $\langle R_{dAu}^{\gamma} \rangle_{\text{MB}}$.

Another interesting feature of figure 4.7 is that the leading order and next-to-leading order calculations of $\langle R_{dAu}^{\pi^0} \rangle_{\text{MB}}$ with EPS09 are very similar. It indicates that $\langle R_{dAu}^{\pi^0} \rangle_{\text{MB}}$ can be calculated to a good precision at leading order.³

It should be noted that the same parameters that are used to calculate equation 4.14 are used for the calculation of the proton-proton cross-section, the denominator of equation 4.11. This of course means same choice of $\alpha_s(M_Z)$, f.f. and so on. For the p.d.f.'s, it means that the p.d.f.'s used for the proton-proton calculations are the reference p.d.f.'s⁴ that were used in the fitting of the nuclear p.d.f.'s. This means CTEQ6.1 for EPS09. For HKN07, there is a subtlety. The reference p.d.f. of HKN07 is MRST98 [51]. However, HKN07 treats heavy quarks in a different manner than MRST98. A proton p.d.f. based on MRST98 but slightly different is thus included with HKN07,

³This is only an interesting, though widely known, observation. All calculations of $\langle R_{dAu} \rangle_{\text{MB}}$ were still made at NLO.

⁴Nuclear p.d.f.'s are generally parametrised as a factor times a proton p.d.f.: $F_{a/A}(x, Q) = R_{a/A}(x, Q)f_{a/p}(x, Q)$. (nDS uses a different approach) It was shown in [46] that $R_{a/A}(x, Q)$ seemed only “moderately sensitive” to the choice of reference proton p.d.f., and it became quite common to use $R_{a/A}(x, Q)$ with different p.d.f.'s than the reference one. This seems to be an unnecessary approximation, however, and here nuclear p.d.f.'s are always used with their reference p.d.f.

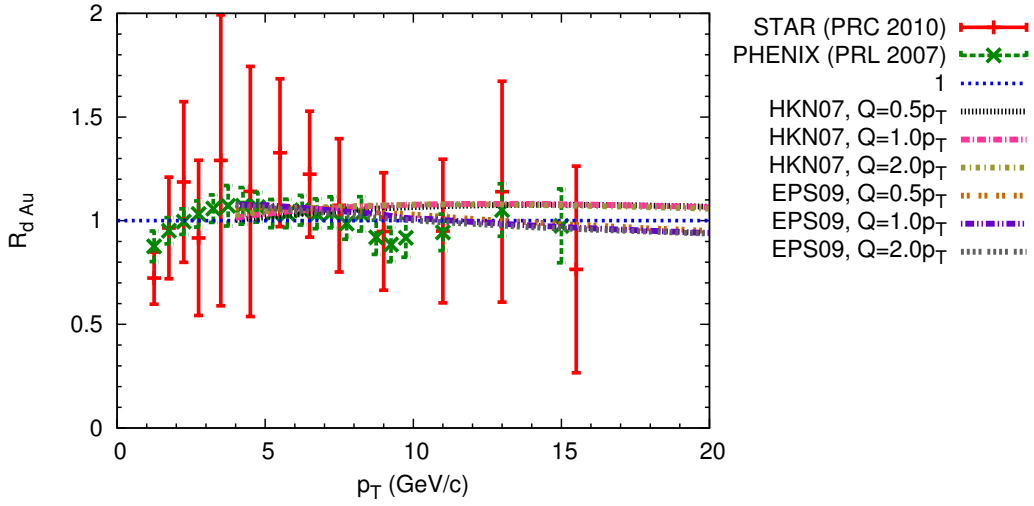


Figure 4.8: $\langle R_{dAu} \rangle_{MB}$ for π^0 compared to calculations with HKN07 and EPS09 nuclear p.d.f.'s. HKN07 corresponds to the upper three curves (at high p_T^0), EPS09 to the lower ones

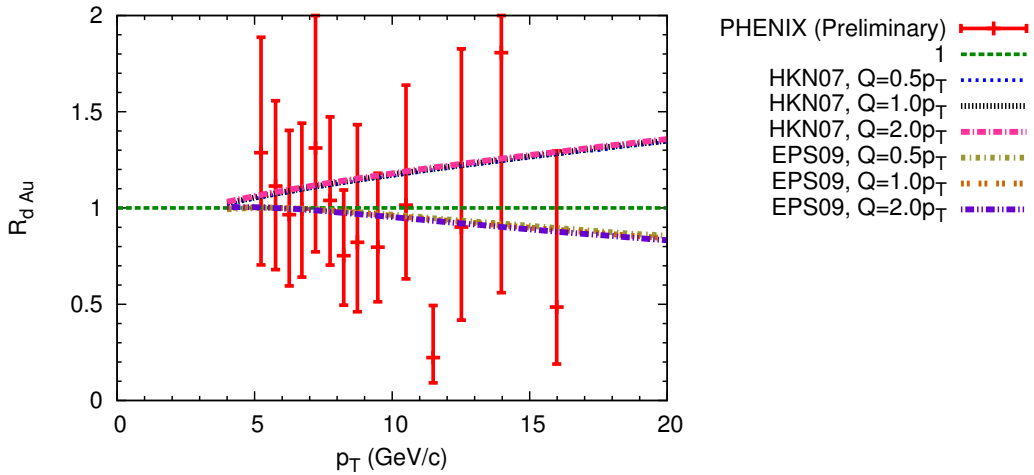


Figure 4.9: $\langle R_{dAu} \rangle_{MB}$ for photons compared to calculations with HKN07 and EPS09 nuclear p.d.f.'s. HKN07 corresponds to the upper three curves, EPS09 to the lower ones

and this is the p.d.f. that was used to calculate the proton-proton cross-section when HKN07 was used as nuclear p.d.f.⁵

The isospin effect is not taken into account in the same way for EPS09 and HKN07. It is already included in HKN07, while it must be added to EPS09.

Results are presented in figures 4.8 and 4.9.⁶ For π^0 , at lower $p_T^{\pi^0}$, calculations with EPS09 are in good agreement with data. For HKN07, the agreement is not as good as for EPS09 in the lower $p_T^{\pi^0}$ but is still reasonable. Neither calculation reproduces the apparent suppression around $p_T^{\pi^0} = 9$ GeV/c, although the calculations with EPS09 does slightly decrease as $p_T^{\pi^0}$ increases. The trend for HKN07 is the opposite, it slightly increases with $p_T^{\pi^0}$. This difference causes the calculations to diverge from each other in the higher range of $p_T^{\pi^0}$, but the uncertainties on the data are too large to tell if one parametrisation of nuclear effects is better than the other.

For photons, both calculations are almost equal at the lowest p_T^γ (around 4 GeV/c) but they diverge from each other as p_T^γ increases. At $p_T^\gamma \approx 20$ GeV/c, the calculation with HKN07 is about 60% larger than the calculation using EPS09. The origin of this surprising disagreement of the calculations has not been identified. The uncertainties on the data are currently too large to tell if one calculation agrees better with the data than the other.

It is not surprising that no conclusion can be drawn from the photon calculations, but interestingly it is also difficult to conclude anything from the π^0 calculations despite the significantly smaller uncertainties on the data. The main reason is that the deviations of $\langle R_{dAu}^{\pi^0} \rangle_{\text{MB}}$ from 1 are small with respect to the uncertainties on the data and to the effect of the nuclear p.d.f.'s on the calculations, which are both of the order of 10%. To some extent, using nuclear p.d.f.'s does seem to lead to some enhancement at small $p_T^{\pi^0}$, but there is no sign of a suppression around 9 GeV/c. It thus cannot be concluded that adding nuclear effects through nuclear p.d.f.'s improves the agreement of the calculations with the data.

There can be many explanations for that conclusion. A first one is that the uncertainties on the calculations (exemplified by the difference in the calculations made with different nuclear p.d.f.'s) and on the data are simply too large to really expect them to agree perfectly. Assuming the values of the data points and the calculations to be reliable, another obvious explanation is that

⁵I thank Dr Masanori Hirai and Shunzo Kumano for their help with that matter.

⁶Reference [49] contains a figure (figure 11) almost identical to figure 4.8 but with error bars on the EPS09 calculation.

nuclear p.d.f.'s are actually not universal and that the approach is intrinsically flawed. A third possibility, that is investigated in the next chapter, is that nuclear p.d.f.'s do not take into account all possible nuclear effects and more ingredients need to be added to the model to describe the data.

The next chapter is devoted to a very specific type of nuclear effects, that is assumed not to be included into nuclear p.d.f.'s: parton energy loss in cold matter.

Chapter 5

Hard parton energy loss in deuteron-gold collisions

In the previous chapters, it was shown that the single-particle inclusive differential cross-sections for photons and π^0 in proton-proton collisions can be well-described by a pQCD-based formula, [equation 2.8](#). It was then showed that even if no pQCD-based formula is known to calculate the same quantity in nucleus-nucleus collisions, a model based on the proton-proton formula and on binary scaling can reproduce well the single-particle inclusive differential cross-sections for photons and π^0 in deuteron-gold collisions. It was shown in [figure 4.5](#), however, that by looking at the nuclear modification factor instead of the cross-section, π^0 data suggests a possible disagreement of the data with simple binary-scaled predictions. It was assumed that nuclear effects could be at the origin of this disagreement, but the inclusion of nuclear effects with nuclear p.d.f.'s did not lead to significant improvements.

The hypothesis investigated in this final chapter is that if the agreement of data with the calculations is not satisfactory, it is because further nuclear effects need to be taken into account. Parton energy loss in cold matter is the additional effect that is studied here.

Parton energy loss is a well-known phenomenon in heavy ion physics. It is easier to use the parton model, which was mentioned in the introduction, to describe what “parton energy loss” means in a nucleus-nucleus collision. [Figure 5.1](#) represents a hadron-hadron and a nucleus-nucleus collision according to the parton model. The picture of the hadron-hadron collision describes just the same thing as [figure 1.2](#) in the introduction: a parton from each hadron interacts, then propagates and fragments. Nucleus-nucleus collisions are very

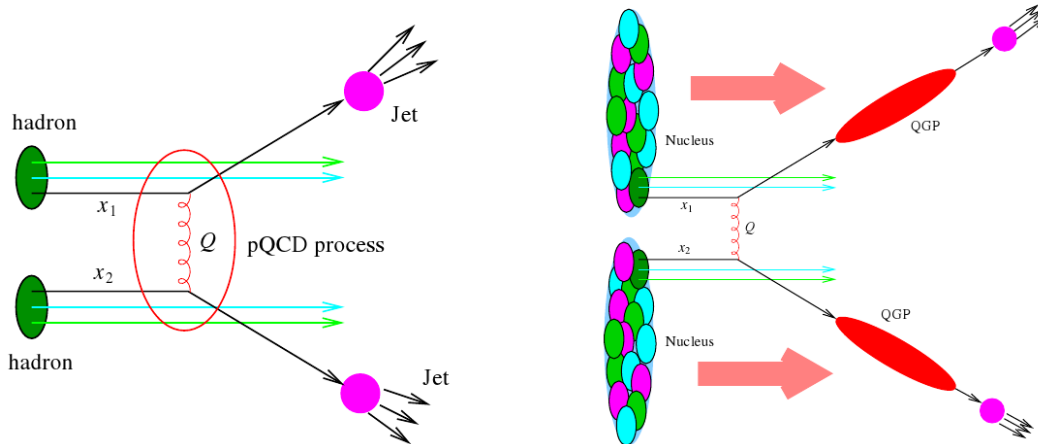


Figure 5.1: Schematic comparison of hadron-hadron (left) and nucleus-nucleus (right) collisions. Figure from [52, Figure 1]

similar, but figure 5.1 points out an important difference: between the initial hard interaction of the partons (the momentum Q exchange) and the fragmentation, the partons no longer propagate in the vacuum, they now interact with the quark-gluon plasma. The results of this interaction is an energy loss for the partons, which is reflected in the energy of the detected jets and hadrons. This is called “jet quenching”.¹

A deuteron-gold collision is not a heavy ion collision. In particular, no QGP is created, at least not at centre-of-mass energies of a few hundred GeV. Energy loss is still possible, however, as interaction with the QGP is not the only way for partons to lose energy, they can also interact with the cold nuclear matter.² For hadron-nucleus collisions, the “cold nuclear matter” basically means the partons of the nucleus [53, Section IV].

To study the influence of energy loss in deuteron-gold collisions, it is possible to use the tools developed to study parton energy loss in heavy ion collisions, a field of research that is very active. The usual framework is to use the

¹More precisely, the term “jet quenching” refers to the experimental observation that proportionally less hard jets are detected in heavy ion collisions than in proton-proton collisions. Parton energy loss is the mainstream theoretical explanation for this observation, but it is not ruled out that other phenomena play a role, maybe small, in jet quenching in heavy ion collisions.

²It should be noted that although parton energy loss is the only hypothesis studied here, there are many other hypotheses, depending on the process and the kinematic range under investigation, that can explain jet quenching *in cold matter*. See [53, Section I]. In particular, hadron energy loss may play a role.

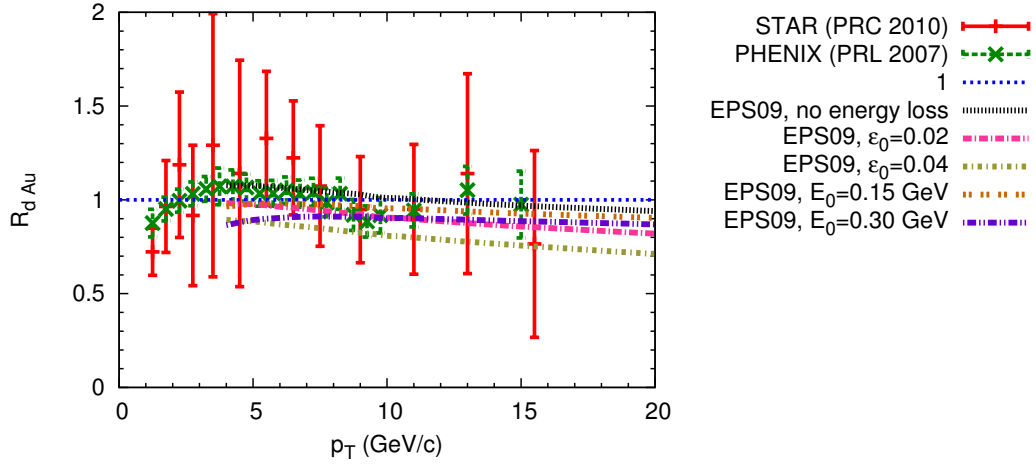


Figure 5.2: $\langle R_{dAu} \rangle_{MB}$ for π^0 calculated with EPS09 nuclear p.d.f. and simple parton energy loss

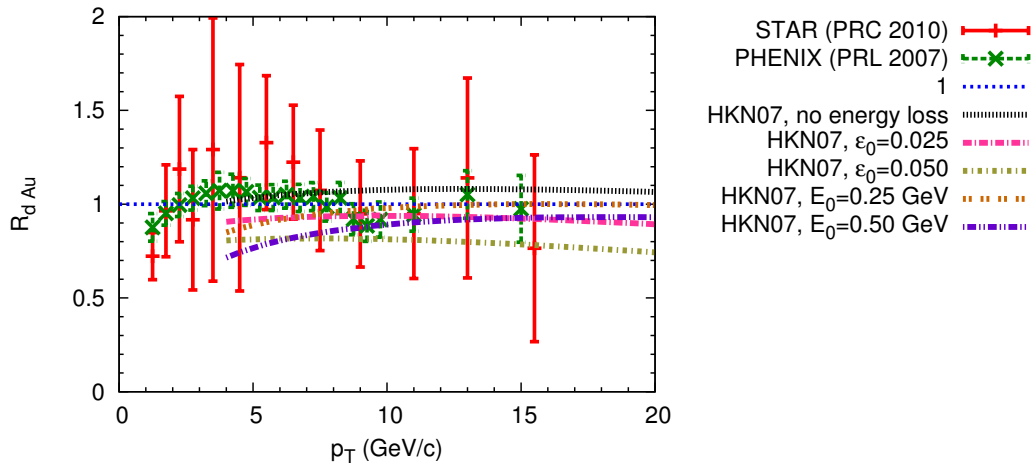


Figure 5.3: $\langle R_{dAu} \rangle_{MB}$ for π^0 calculated with HKN07 nuclear p.d.f. and simple parton energy loss

following formula for the cross-section with energy loss:

$$\left\langle E_h \frac{d^3\sigma_{AB}^{\text{inel}}}{dp_h^3} \right\rangle_{\text{MB}} = AB \sum_{a,b,c} \int dx_a dx_b \frac{dz_c}{z_c} F_{a/A}(x_a, Q_{\text{fac}}) F_{b/B}(x_b, Q_{\text{fac}}) \times \left[E_c \frac{d^3\hat{\sigma}}{dk_c^3}(Q_{\text{ren}}) \right] \tilde{D}_{h/c}(z_c, Q_{\text{frag}}) \quad (5.1)$$

This formula is basically [equation 4.10](#) with a medium-modified fragmentation function, $\tilde{D}_{h/c}(z, Q)$, in which all effects of final state parton energy loss are assumed to be absorbed. Various models have been developed to describe parton energy loss in QGP. A review of the main ones is presented in [54, Section 3]. Some of these models are expected to be applicable to cold matter energy loss, or even to work better in that case [55, Section 6.3]. However, those models are very complex and a simpler approach is taken here.

5.1 Simple model of parton energy loss

As a simple model of parton energy loss, it is assumed that every parton loses a fraction ϵ_0 or an absolute amount E_0 of its energy as it interacts with the cold matter. The medium-modified fragmentation function for this model is

$$\tilde{D}_{h/c}(z, Q) = \frac{1}{1 - \epsilon_0} D_{h/c} \left(\frac{z}{1 - \epsilon_0}, Q \right) \quad (5.2)$$

or

$$\tilde{D}_{h/c}(z, Q, E_i) = \frac{1}{1 - E_0/E_i} D_{h/c} \left(\frac{z}{1 - E_0/E_i}, Q \right) \quad (5.3)$$

where E_i is the energy of the parton immediately after the hard collision.³

The above model is too simple to realistically describe parton energy loss, but it is a good starting point and it can give a rough idea of the effect of parton energy loss on hard particle production. Results are presented in figures 5.2 and 5.3 for π^0 and in figures 5.4 and 5.5 for photons, for various values of ϵ_0 and E_0 . The values were set with respect to the π^0 data, and were used for both photons and π^0 . Different values were used for EPS09 (figures 5.2 and 5.4) and HKN07 (figures 5.3 and 5.5). For clarity, only one choice of scales is

³This simple approach can be seen as a simplification of the “quenching weights” energy loss models where the modified fragmentation function is $\tilde{D}(z, Q) = \int_0^{(1-z)E_i} dE \mathcal{P}(E) \frac{1}{1-E/E_i} D \left(\frac{z}{1-E/E_i}, Q \right)$. The quenching weight $\mathcal{P}(E)$ is an “energy loss probability distributions” [55, Section 6.2]. The model used here is equivalent to using the oversimplified probability distributions $\mathcal{P}(E) = \delta(E - \epsilon_0 E_i)$ and $\mathcal{P}(E) = \delta(E - E_0)$.

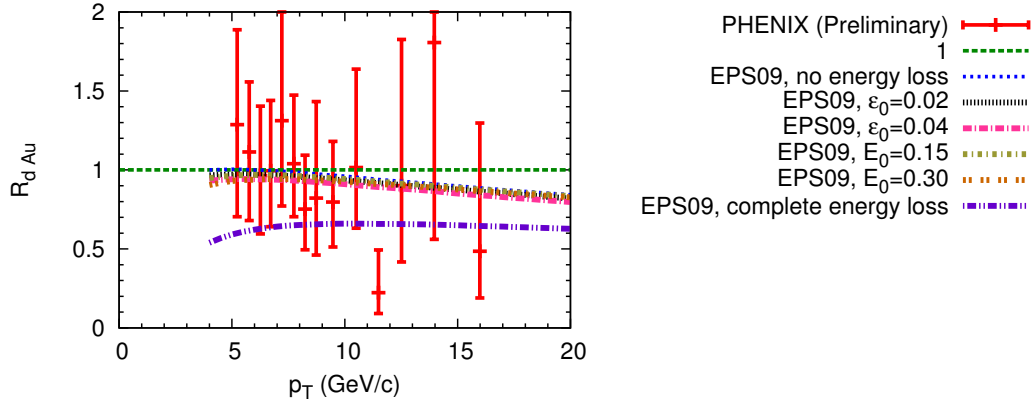


Figure 5.4: $\langle R_{dAu} \rangle_{MB}$ for photons calculated with EPS09 nuclear p.d.f. and simple parton energy loss

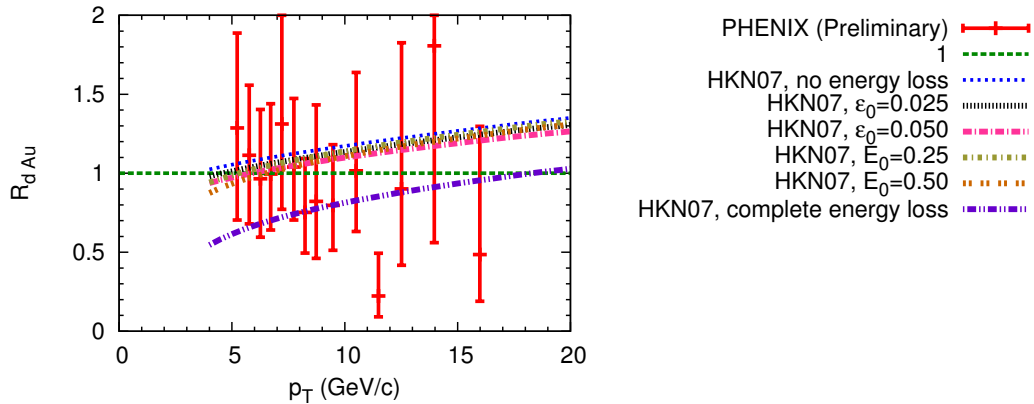


Figure 5.5: $\langle R_{dAu} \rangle_{MB}$ for photons calculated with HKN07 nuclear p.d.f. and simple parton energy loss

shown, $Q_{\text{fac}} = Q_{\text{ren}} = Q_{\text{frag}} = p_T$.

It can be seen for π^0 data that a relative energy loss (equation 5.2) has very little effect on the shape of the calculations, it mainly changes the normalisation of $\langle R_{dAu} \rangle_{\text{MB}}$. On the other hand, an absolute energy loss (equation 5.3) suppresses $\langle R_{dAu} \rangle_{\text{MB}}$ much more at low p_T than at higher p_T .

The values of energy loss that seem reasonable for π^0 result in a very small effect of energy loss on the photon $\langle R_{dAu} \rangle_{\text{MB}}$. This could be expected as isolated photons, which contribute significantly to the photon cross-section, are unaffected by parton energy loss. The curves labelled “complete energy loss” in figures 5.4 and 5.5 illustrate this fact: they represent $\langle R_{dAu} \rangle_{\text{MB}}$ assuming no contribution from fragmentation photons to the deuteron-gold cross-sections, that is, a 100% parton energy loss. To some extent, this can be seen as a lower limit to parton energy loss. The fact that the uncertainties on photon data include those lower limit curves on almost the whole range of p_T^γ is a good indication of how little information on energy loss can be obtained from the present data.

In the case of the better π^0 data, it is not clear that energy loss can improve the agreement of the calculations with data. Actually, it depends on the range of $p_T^{\pi^0}$ that is looked at. Before even looking at this, however, it is interesting to compare the proposed amount of energy loss with a more realistic extraction of energy loss based on experimental data.

5.2 Comparison with another model of energy loss

It is possible to relate parton energy loss in hadron-nucleus collisions to parton energy loss of a similar observable in another process: jet or hadron production in electron-nucleus collisions. This observable can be called nuclear semi-inclusive deep-inelastic scattering (nSIDIS) in reference to semi-inclusive deep-inelastic scattering (SIDIS), the observable where jet or hadron production is studied in electron-hadron collisions. Figure 5.6 illustrates how parton energy loss is related in nSIDIS and hadron-nucleus collisions. On the left is illustrated a parton propagating in a nucleus, then undergoing a hard interaction, propagating out of the nucleus and finally fragmenting into hadrons. It represents the production of a jet in a hadron-nucleus collision. The process

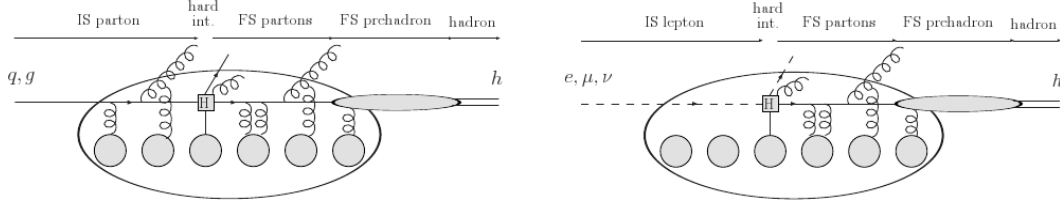


Figure 5.6: Diagrammatic comparison of hadron-nucleus collisions (left) and semi-inclusive nuclear deep-inelastic scattering (right). Figure modified from [55, Figure 43]

on the right, which describes a nSIDIS, is the same except that it is an electron instead of a parton that propagates *in* the nucleus.

According to figure 5.6, the difference between the two processes is what happens before the hard collision (denoted by an “H” on the figure). This is because in a nucleus-nucleus collision the incoming parton has a large probability of interacting with the nucleus *before* the hard collision, while this probability is very small for the incoming electron in nSIDIS. The interactions happening before the hard collision are called “initial state effects”. Those happening after the hard collision are called “final state effects”, which means that parton energy loss is a final state effect.

Figure 5.6 shows that final state effects should be the same in nSIDIS and hard particle production in nuclear-nuclear collisions, which is why it should be possible to compare parton energy loss from those processes. This approach is exactly the one used in [53]: using a more advanced model of energy loss than what was used in the previous section and a value of cold matter energy loss extracted from nSIDIS data, R_{dAu} with parton energy loss is calculated, *with no free parameter*⁴, for charged pions at various rapidities. The midrapidity calculation is shown in figure 5.7a.

It is possible to compare the parton energy loss shown in figure 5.7a to a calculation made with equation 5.3 as modified f.f. by simple graphical comparison, that is by finding the value of E_0 that reproduces figure 5.7a as well as possible. Equation 5.3 is chosen over equation 5.2 as it reproduces better the shape of the curve of figure 5.7a. The parameters used for the comparison are the same as in section 4.3 except that no nuclear p.d.f. is used

⁴All the free parameters are fixed experimentally or related to others by models. This absence of free parameters thus probably comes with a heavy model dependence.

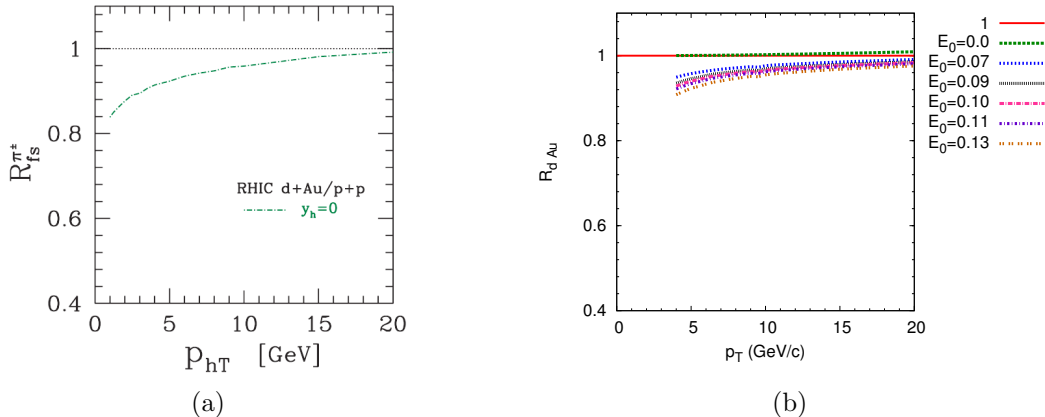


Figure 5.7: Comparison of the result of [53] (left) and calculations of energy loss with equation 5.3 as medium modified fragmentation function (right). See text for details. Figure 5.7a modified from [53, Figure 6]

as none is used in [53].⁵

As illustrated in figure 5.7, the calculation of [53] is contained on most of the $p_T^{\pi^0}$ range between the calculations made with equation 5.3 using $E_0 = 0.07$ and 0.13 GeV, with a middle value of $E_0 \approx 0.1$ GeV. As the calculation of [53] is related to nSIDIS results, a value of $E_0 \approx 0.1$ GeV can be viewed as an estimate of E_0 extracted, although quite indirectly, from a measurement of parton energy loss in nSIDIS. This extraction is very approximative, but it is able to constrain the magnitude of E_0 to realistic values.

5.3 Analysis

As mentioned before, using equation 5.2 as medium-modified f.f. does not modify significantly the shape of $\langle R_{dAu} \rangle_{MB}$. The more advanced model of energy loss in [53] has a similar effect as equation 5.3, that is, it suppresses lower $p_T^{\pi^0}$ more than higher ones. The effect is monotonical and smooth, however, and cannot explain the suppression hinted by π^0 data at $p_T^{\pi^0} \gtrsim 9$ GeV/c.

The extraction of E_0 in the previous section does suggest that there should be a small but noticeable parton energy loss in deuteron-gold collisions. Indeed, an energy loss corresponding to $E_0 \approx 0.1$ GeV is roughly the maximum parton energy loss that the deuteron-gold data under study seem to be able to ac-

⁵Unfortunately, the choice of p.d.f., f.f., scales and so on is not clearly specified in [53]. As they have little effect on the *nuclear modification factor* (since they enter in both the numerator and the denominator), this is not expected to be a problem, however.

commodate. This can be inferred from the low $p_T^{\pi^0}$ data ($p_T^{\pi^0} \approx 4$ to 9 GeV/ c), which have the smallest uncertainties. With an energy loss of $E_0 \approx 0.1$ GeV, the EPS09 calculation would still be within the experimental uncertainties, but the HKN07 calculation would graze the lower boundary of the uncertainties, or would be slightly below them. Energy loss in nSIDIS and deuteron-gold collisions thus seem to be marginally compatible, or there may even be a hint of disagreement, but it is clear that further comparisons with better models of parton energy loss and improved comparisons with nSIDIS data are required.⁶

The question of the possible improvement of the agreement of calculations with data by the addition of energy loss is interesting, but the answer is very speculative. According to the simple model used, the addition of energy loss, be it $E_0 \approx 0.1$ GeV or larger, does not improve the overall agreement with data. The trend of the data at $p_T^{\pi^0} > 9$ GeV/ c agrees better with calculations that include a fairly large energy loss ($E_0 \approx 0.3$ – 0.5 GeV), but this comes with a complete disagreement with the lower $p_T^{\pi^0}$ data. If new data confirm this increasing trend at high $p_T^{\pi^0}$, it would be interesting to investigate this effect further. In the absence of such an incentive, however, there seems to be little reason, according to the results obtained here, to expect that calculations of $\langle R_{dAu} \rangle_{\text{MB}}$ can be improved by adding parton energy loss. This conclusion will have to be verified by other studies with better models of energy loss.

⁶The assumption that parton energy loss is not included in nuclear p.d.f.'s may also be questioned. If it turns out that the effect of energy loss is already, in part or completely, included in nuclear p.d.f.'s, using both nuclear p.d.f.'s and a value of energy loss extracted from nSIDIS would account twice for the same effect.

Chapter 6

Conclusion

Leading twist, next-to-leading order calculations of hard photon and π^0 cross-sections in proton-proton collisions were shown to agree very well with data measured at RHIC. Hard photon and π^0 cross-sections in deuteron-gold collisions, also measured at RHIC, were shown to be well described by a model based on the optical Glauber model and the formula used for proton-proton cross-sections. Calculating $\langle R_{dAu} \rangle_{\text{MB}}$ showed, however, that there may be a small but noticeable disagreement of the calculations with data, at least for π^0 . Neither the use of nuclear parton distribution functions nor the addition of parton energy loss in cold matter through a simple model succeeded in significantly improving the agreement of $\langle R_{dAu} \rangle_{\text{MB}}$ with data. The comparison of parton energy loss in deuteron-gold collisions with that of electron-nucleus collisions was inconclusive.

A key ingredient that is missing everywhere in this work is theoretical uncertainties. All the above conclusions are drawn from comparisons of theoretical calculations without uncertainties against data with uncertainties¹. If theoretical uncertainties were added, it is likely that some conclusions would have to be modified. Adding theoretical uncertainties is not a simple task, not even for cross-sections in proton-proton collisions. But as seen in the fourth chapter, deviations of $\langle R_{dAu} \rangle_{\text{MB}}$ from binary scaling are small, below 10%, and uncertainties larger than that are quite possible. If theoretical uncertainties turn out to be large, it may not be worthwhile to try to improve the agreement of $\langle R_{dAu} \rangle$ with data by adding additional ingredients like parton energy loss to the calculation; it might be wiser to try to lower the uncertainties, or to try a different approach.

¹Modulo normalisation uncertainties.

On the other hand, if uncertainties are well under control, it would be very interesting to see what ingredients are needed to better describe $\langle R_{dAu} \rangle$. It would also be of interest to see whether or not binary scaling is the best starting point, or if the pQCD-based formulae for hadron-hadron collisions can be extended to hadron-nucleus and nucleus-nucleus collisions. Or if a semi-phenomenological approach using nuclear p.d.f.'s is actually that good of an idea. Even parton energy loss, which seems unlikely to be the only missing ingredient according to the results of this thesis, might still be an important one. If this turns out to be the case, studying cold matter energy loss might prove to be a much better testing ground for energy loss formalisms than heavy ion collisions.

Fresh results from the Large Hadron Collider may provide answers to some of these questions; actually, the kinematic range probed at the LHC is so different from RHIC's that the new data may even provide answers without any calculations of theoretical uncertainties. As far as RHIC is concerned, however, the future of studies of $\langle R_{dAu} \rangle$ seems to hinge critically on reliable estimates of theoretical uncertainties.

Bibliography

- [1] M. K. Gaillard, P. D. Grannis, and F. J. Sciulli, “The standard model of particle physics,” *Reviews of Modern Physics*, vol. 71, p. S96, Mar 1999.
- [2] H. W. Kendall, “Deep inelastic scattering: Experiments on the proton and the observation of scaling,” *Reviews of Modern Physics*, vol. 63, pp. 597–614, Jul 1991.
- [3] M. Klein and R. Yoshida, “Collider physics at HERA,” *Progress in Particle and Nuclear Physics*, vol. 61, no. 2, pp. 343–393, 2008.
- [4] P. Braun-Munzinger and J. Stachel, “The quest for the quark–gluon plasma,” *Nature*, vol. 448, no. 7151, pp. 302–309, 2007.
- [5] G. C. Fox and S. Wolfram, “Event shapes in e^+e^- annihilation,” *Nuclear Physics B*, vol. 149, no. 3, pp. 413–496, 1979.
- [6] C. Burgess and G. Moore, *The Standard Model: A primer*. Cambridge University Press, 2007.
- [7] M. E. Peskin and D. V. Schroeder, *An Introduction to Quantum Field Theory*. Westview Press, 1995.
- [8] J. C. Collins, *The Foundations of Perturbative QCD*. 2010. (draft).
- [9] S. Bethke, “The 2009 world average of α_S ,” *The European Physical Journal C*, vol. 64, pp. 689–703, 2009.
- [10] K. Nakamura *et al.*, “Review of Particle Physics,” *Journal of Physics G*, vol. 37, p. 075021, 2010.
- [11] G. Sterman, J. Smith, J. C. Collins, J. Whitmore, R. Brock, J. Huston, J. Pumplin, W.-K. Tung, H. Weerts, C.-P. Yuan, S. Kuhlmann, S. Mishra, J. G. Morfin, F. Olness, J. Owens, J. Qiu, and D. E. Soper, “Handbook

- of perturbative QCD,” *Reviews of Modern Physics*, vol. 67, pp. 157–248, Jan 1995.
- [12] T. Wyatt, “High-energy colliders and the rise of the standard model,” *Nature*, vol. 448, pp. 274–280, 2007.
- [13] E. Laenen and D. Wackerth, “Radiative Corrections for the LHC and Linear Collider Era,” *Annual Review of Nuclear and Particle Science*, vol. 59, no. 1, pp. 367–396, 2009.
- [14] D. de Florian and W. Vogelsang, “Threshold resummation for the inclusive-hadron cross section in pp collisions,” *Physical Review D*, vol. 71, p. 114004, Jun 2005.
- [15] J. C. Collins and D. E. Soper, “The theorems of perturbative QCD,” *Annual Review of Nuclear and Particle Science*, vol. 37, no. 1, pp. 383–409, 1987.
- [16] J. C. Collins, D. E. Soper, and G. F. Sterman, “Factorization of Hard Processes in QCD,” *Advanced Series on Directions in High Energy Physics*, vol. 5, pp. 1–91, 1988. (arXiv:hep-ph/0409313v1).
- [17] J. C. Collins, “Hard-scattering factorization with heavy quarks: A general treatment,” *Physical Review D*, vol. 58, p. 094002, Sep 1998.
- [18] R. S. Thorne and W. K. Tung, “PQCD Formulations with Heavy Quark Masses and Global Analysis,” 2008. (arXiv:0809.0714v2).
- [19] P. M. Nadolsky and W.-K. Tung, “Improved formulation of global QCD analysis with zero-mass hard cross sections,” *Physical Review D*, vol. 79, p. 113014, Jun 2009.
- [20] J. F. Owens, “Large-momentum-transfer production of direct photons, jets, and particles,” *Reviews of Modern Physics*, vol. 59, no. 2, pp. 465–503, 1987.
- [21] R. Cutler and D. Sivers, “Quantum-chromodynamic gluon contributions to large- p_T reactions,” *Physical Review D*, vol. 17, pp. 196–211, Jan 1978.
- [22] J. Pumplin, D. R. Stump, J. Huston, H. L. Lai, P. Nadolsky, and W. K. Tung, “New generation of parton distributions with uncertainties from

- global QCD analysis,” *Journal of High Energy Physics*, vol. 2002, p. 012, 2002.
- [23] B. A. Kniehl, G. Kramer, and B. Pötter, “Fragmentation functions for pions, kaons, and protons at next-to-leading order,” *Nuclear Physics B*, vol. 582, no. 1–3, pp. 514–536, 2000.
- [24] S. Albino, B. A. Kniehl, and G. Kramer, “Fragmentation functions for light charged hadrons with complete quark flavour separation,” *Nuclear Physics B*, vol. 725, no. 1–2, pp. 181–206, 2005.
- [25] S. Albino, B. A. Kniehl, and G. Kramer, “AKK update: Improvements from new theoretical input and experimental data,” *Nuclear Physics B*, vol. 803, no. 1–2, pp. 42–104, 2008.
- [26] L. Bourhis, M. Fontannaz, and J. P. Guillet, “Quark and gluon fragmentation functions into photons,” *The European Physical Journal C*, vol. 2, no. 3, pp. 529–537, 1998.
- [27] PHENIX Collaboration, “Inclusive cross section and double helicity asymmetry for π^0 production in $p+p$ collisions at $\sqrt{s} = 200 \text{ GeV}$: Implications for the polarized gluon distribution in the proton,” *Physical Review D*, vol. 76, p. 051106, Sep 2007.
- [28] PHENIX Collaboration, “Centrality Dependence of π^0 and η Production at Large Transverse Momentum in $\sqrt{s_{NN}} = 200 \text{ GeV}$ $d + Au$ Collisions,” *Physical Review Letters*, vol. 98, p. 172302, Apr 2007.
- [29] STAR Collaboration, “Longitudinal double-spin asymmetry and cross section for inclusive neutral pion production at midrapidity in polarized proton collisions at $\sqrt{s} = 200 \text{ GeV}$,” *Physical Review D*, vol. 80, p. 111108, Dec 2009.
- [30] P. Stankus, “Direct Photon Production in Relativistic Heavy-Ion Collisions,” *Annual Review of Nuclear and Particle Science*, vol. 55, pp. 517–554, 2005.
- [31] PHENIX Collaboration, “Detailed measurement of the e^+e^- pair continuum in $p+p$ and $Au + Au$ collisions at $\sqrt{s_{NN}} = 200 \text{ GeV}$ and implications for direct photon production,” *Physical Review C*, vol. 81, p. 034911, Mar 2010.

- [32] PHENIX Collaboration, “Measurement of Direct Photon Production in $p + p$ Collisions at $\sqrt{s} = 200 \text{ GeV}$,” *Physical Review Letters*, vol. 98, p. 012002, Jan 2007.
- [33] STAR Collaboration, “Inclusive π^0 , η , and direct photon production at high transverse momentum in $p + p$ and $d + Au$ collisions at $\sqrt{s_{NN}} = 200 \text{ GeV}$,” *Physical Review C*, vol. 81, p. 064904, Jun 2010.
- [34] P. Aurenche, R. Baier, M. Fontannaz, and D. Schiff, “Prompt Photon Production at Large p_T Scheme Invariant QCD Predictions and Comparison with Experiment,” *Nuclear Physics B*, vol. 297, p. 661, 1988.
- [35] F. Aversa, P. Chiappetta, M. Greco, and J. P. Guillet, “QCD Corrections to Parton-Parton Scattering Processes,” *Nuclear Physics B*, vol. 327, p. 105, 1989.
- [36] G. Rodrigo and A. Santamaria, “QCD matching conditions at thresholds,” *Physics Letters B*, vol. 313, no. 3–4, pp. 441–446, 1993.
- [37] D. Stump, J. Huston, J. Pumplin, W. K. Tung, H. L. Lai, S. Kuhlmann, and J. F. Owens, “Inclusive jet production, parton distributions, and the search for new physics,” *Journal of High Energy Physics*, vol. 2003, p. 046, 2003.
- [38] M. L. Miller, K. Reygers, S. J. Sanders, and P. Steinberg, “Glauber Modeling in High-Energy Nuclear Collisions,” *Annual Review of Nuclear and Particle Science*, vol. 57, no. 1, pp. 205–243, 2007.
- [39] NA50 Collaboration, “Charmonia and Drell-Yan production in proton-nucleus collisions at the CERN SPS,” *Physics Letters B*, vol. 553, no. 3–4, pp. 167–178, 2003.
- [40] PHENIX Collaboration, “Absence of Suppression in Particle Production at Large Transverse Momentum in $\sqrt{s_{NN}} = 200 \text{ GeV}$ $d + Au$ Collisions,” *Physical Review Letters*, vol. 91, no. 7, p. 72303, 2003.
- [41] D. Peressounko for the PHENIX collaboration, “Direct Photon Production in $p + p$ and $d + Au$ Collisions Measured with the PHENIX Experiment,” *Nuclear Physics A*, vol. 783, no. 1–4, pp. 577–582, 2007.

- [42] D. d’Enterria, “Hard scattering cross sections at LHC in the Glauber approach: from pp to pA and AA collisions,” 2004. (arXiv:nucl-ex/0302016v3).
- [43] S. N. White, “Diffraction dissociation — 50 years later,” *AIP Conference Proceedings*, vol. 792, pp. 527–531, 2005.
- [44] T. Sakaguchi for the PHENIX Collaboration, “PHENIX photons and dileptons,” 2010. (arXiv:1012.1893v1).
- [45] CERN’s PDFs, Shadowing and p+A Working Group, “Hard probes in heavy ion collisions at the LHC: PDFs, shadowing and pA collisions,” 2004. (arXiv:hep-ph/0308248).
- [46] K. J. Eskola, V. J. Kolhinen, and C. A. Salgado, “The Scale dependent nuclear effects in parton distributions for practical applications,” *The European Physical Journal C*, vol. 9, no. 1, pp. 61–68, 1999.
- [47] D. De Florian and R. Sassot, “Nuclear parton distributions at next to leading order,” *Physical Review D*, vol. 69, no. 7, p. 74028, 2004.
- [48] M. Hirai, S. Kumano, and T.-H. Nagai, “Determination of nuclear parton distribution functions and their uncertainties at next-to-leading order,” *Physical Review C*, vol. 76, p. 065207, Dec 2007.
- [49] K. J. Eskola, H. Paukkunen, and C. A. Salgado, “EPS09 — A new generation of NLO and LO nuclear parton distribution functions,” *Journal of High Energy Physics*, vol. 2009, p. 065, 2009.
- [50] P. Quiroga-Arias, J. G. Milhano, and U. A. Wiedemann, “Testing nuclear parton distributions with pA collisions at the TeV scale,” *Physical Review C*, vol. 82, p. 034903, 2010.
- [51] A. D. Martin, R. G. Roberts, W. J. Stirling, and R. S. Thorne, “Parton distributions: A New global analysis,” *The European Physical Journal C*, vol. 4, no. 3, pp. 463–496, 1998.
- [52] S. Jeon, “Jet Quenching in Evolving QGP Medium,” *Nuclear Physics A*, vol. 830, no. 1–4, pp. 107c–114c, 2009.
- [53] A. Accardi, “Final state interactions and hadron quenching in cold nuclear matter,” *Physical Review C*, vol. 76, no. 3, p. 34902, 2007.

- [54] D. Enterria and B. Betz, “High- p_T Hadron Suppression and Jet Quenching,” in *The Physics of the Quark-Gluon Plasma* (S. Sarkar, H. Satz, and B. Sinha, eds.), vol. 785 of *Lecture Notes in Physics*, pp. 285–339, Springer Berlin / Heidelberg, 2009.
- [55] A. Accardi, F. Arleo, W. K. Brooks, D. D’Enterria, and V. Muccifora, “Parton Propagation and Fragmentation in QCD Matter,” *Rivista del Nuovo Cimento*, vol. 32, pp. 439–553, 2010. (arXiv:0907.3534v1).